Food and Chemical Toxicology 126 (2019) 113–141

Contents lists available at ScienceDirect

Food and Chemical Toxicology

journal homepage: www.elsevier.com/locate/foodchemtox

A six-month systems toxicology inhalation/cessation study in ApoE$^{-/-}$ mice to investigate cardiovascular and respiratory exposure effects of modified risk tobacco products, CHTP 1.2 and THS 2.2, compared with conventional cigarettes

Blaine Phillips[a,1], Justyna Szostak[b,1], Bjoern Titz[b], Walter K. Schlage[c], Emmanuel Guedj[b], Patrice Leroy[b], Gregory Vuillaume[b], Florian Martin[b], Ansgar Buettner[d], Ashraf Elamin[b], Alain Sewer[b], Nicolas Sierro[b], Mohamed Amin Choukrallah[b], Thomas Schneider[b], Nikolai V. Ivanov[b], Charles Teng[a], Ching Keong Tung[a], Wei Ting Lim[a], Ying Shan Yeo[a], Patrick Vanscheeuwijck[b], Manuel C. Peitsch[b], Julia Hoeng[b,*]

[a] PMI R&D, Philip Morris International Research Laboratories Pte. Ltd., Science Park II, Singapore
[b] PMI R&D, Philip Morris Products S.A., Quai Jeanrenaud 5, CH-2000, Neuchâtel, Switzerland
[c] Max-Baermann-Str. 21, 51429, Bergisch Gladbach, Germany
[d] Histovia GmbH, Schöne Aussicht 5, 51491, Overath, Germany

ARTICLE INFO

Keywords:
Cigarette smoking
Lung
Emphysema
Inflammation
Omics
Modified-risk tobacco products (MRTP)

ABSTRACT

Smoking is one of the major modifiable risk factors in the development and progression of chronic obstructive pulmonary disease (COPD) and cardiovascular disease (CVD). Modified-risk tobacco products (MRTP) are being developed to provide substitute products for smokers who are unable or unwilling to quit, to lessen the smoking-related health risks. In this study, the ApoE$^{-/-}$ mouse model was used to investigate the impact of cigarette smoke (CS) from the reference cigarette 3R4F, or aerosol from two potential MRTPs based on the heat-not-burn principle, carbon heated tobacco product 1.2 (CHTP1.2) and tobacco heating system 2.2 (THS 2.2), on the cardiorespiratory system over a 6-month period. In addition, cessation or switching to CHTP1.2 after 3 months of CS exposure was assessed. A systems toxicology approach combining physiology, histology and molecular measurements was used to evaluate the impact of MRTP aerosols in comparison to CS. CHTP1.2 and THS2.2 aerosols, compared with CS, demonstrated lower impact on the cardiorespiratory system, including low to absent lung inflammation and emphysematous changes, and reduced atherosclerotic plaque formation. Molecular analyses confirmed the lower engagement of pathological mechanisms by MRTP aerosols than CS. Both cessation and switching to CHTP1.2 reduced the observed CS effects to almost sham exposure levels.

1. Introduction

Smoking is the leading modifiable risk factor for many human diseases and promotes the initiation as well as the progression of chronic obstructive pulmonary disease (COPD), cardiovascular disease (CVD), and lung cancer (Centers for Disease and Prevention, 2008; Ezzati et al., 2005; Laniado-Laborin, 2009). Smoking cessation is an effective way to reduce the risk of developing smoking-related diseases, such as lung cancer, COPD, and CVD, including myocardial infarction (Attard et al., 2017; Serrano et al., 2003), and is also associated with increased life

* Corresponding author.
E-mail addresses: Blaine.Phillips@pmi.com (B. Phillips), Justyna.Szostak@pmi.com (J. Szostak), Bjorn.Titz@pmi.com (B. Titz), wk.schlage@t-online.de (W.K. Schlage), Emmanuel.Guedj@pmi.com (E. Guedj), Patrice.Leroy@pmi.com (P. Leroy), Gregory.Vuillaume@pmi.com (G. Vuillaume), Florian.Martin@pmi.com (F. Martin), a.buettner@histovia.com (A. Buettner), Ashraf.Elamin@pmi.com (A. Elamin), Alain.Sewer@pmi.com (A. Sewer), Nicolas.Sierro@pmi.com (N. Sierro), MohamedAmin.Choukrallah@pmi.com (M.A. Choukrallah), Thomas.Schneider@pmi.com (T. Schneider), Nikolai.Ivanov@pmi.com (N.V. Ivanov), Charles.Teng@pmi.com (C. Teng), ChingKeong.Tung@pmi.com (C.K. Tung), WeiTing.Lim@pmi.com (W.T. Lim), YingShan.Yeo@pmi.com (Y.S. Yeo), Patrick.Vanscheeuwijck@pmi.com (P. Vanscheeuwijck), Manuel.Peitsch@pmi.com (M.C. Peitsch), Julia.Hoeng@pmi.com (J. Hoeng).
[1] Contributed equally.

https://doi.org/10.1016/j.fct.2019.02.008
Received 23 November 2018; Received in revised form 24 January 2019; Accepted 4 February 2019
Available online 12 February 2019
0278-6915/ © 2019 Published by Elsevier Ltd.

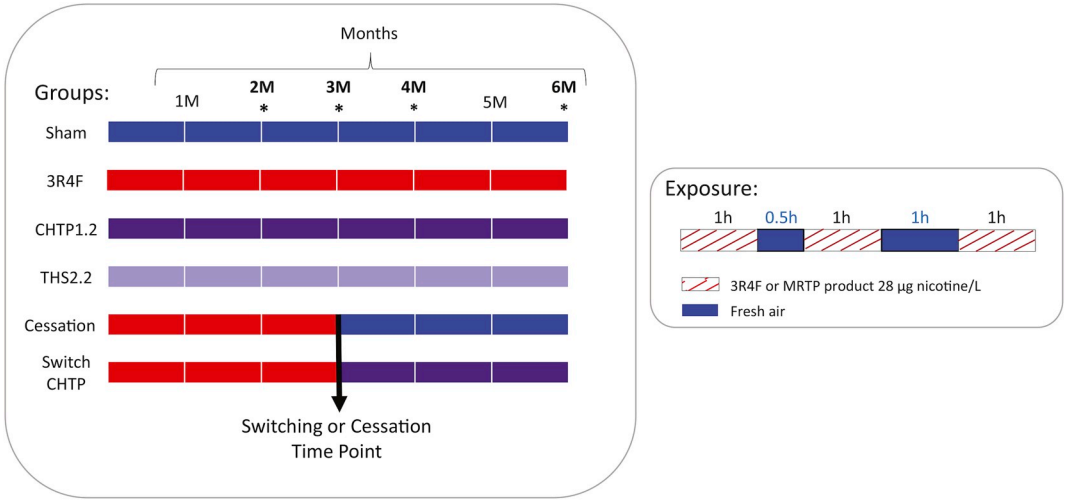

Fig. 1. Study design. Groups and exposure. 3R4F corresponds to the standard reference cigarette; THS 2.2 and CHTP 1.2 correspond to potential MRTP. THS 2.2: Tobacco Heating System 2.2, CHTP 1.2: Carbon Heated Tobacco Product 1.2. Cessation and switching time point takes place at three months and is indicated by the black arrow for corresponding groups. *corresponds to tissue collection time point for systems biology assessment (transcriptomics, proteomics, lipidomics, genomics).

expectancy (Cho et al., 2018; Taylor et al., 2002). Because not all smokers necessarily stop smoking cigarettes, alternative modified-risk tobacco products (MRTP) are being developed to provide substitute products for smokers who are unable or unwilling to quit smoking. The U.S. Food and Drug Administration defines an MRTP as "any tobacco product that is sold or distributed for use to reduce harm or the risk of tobacco-related disease associated with commercially marketed tobacco products" (FDA, 2015; Food and Drug Administration, 2012b). Potential MRTPs, such as heat-not-burn tobacco products, generate reduced yields of toxicants compared with cigarettes and hold great potential for reducing the harms associated with tobacco use (Murphy et al., 2017). Heating rather than burning leads to substantially diminished levels of a harmful and potentially harmful constituents (HPHC) in MRTP aerosols, compared to cigarette smoke. (Tricker et al., 2012, Schaller et al., 2016).

The Carbon Heated Tobacco Product (CHTP) 1.2 and the Tobacco Heating System (THS) 2.2 are two heat-not-burn tobacco products developed by Philip Morris International (PMI). CHTP 1.2 uses a pressed carbon heat source to heat a tobacco plug in a specially designed stick to produce a nicotine-containing aerosol (Phillips et al., 2018). THS 2.2 uses a precisely controlled electric heating device into which a specially designed tobacco product, the Tobacco Stick, is inserted and heated to generate a nicotine-containing aerosol (Smith et al., 2016).

Nonclinical studies may offer useful information about the health risks and abuse liability of a tobacco product (Food and Drug Administration, 2012a). While *in vitro* studies are important for basic toxicity assessment and comparative product testing, animal studies play a fundamental role in analyzing the impact on disease mechanisms. Among the available rodent models, the apolipoprotein E-deficient ($ApoE^{-/-}$) mouse is commonly used in cardiovascular research. $ApoE^{-/-}$ mice spontaneously develop atherosclerotic lesions on a standard chow diet, and these lesions exhibit structural similarity to human atherosclerotic plaques (Lo Sasso et al., 2016). Moreover, $ApoE^{-/-}$ mice present an impaired alveologenesis (Massaro and Massaro, 2008) and develop emphysematous changes (Goldklang et al., 2012). Exposure to cigarette smoke (CS) increases atherosclerotic plaque progression, amplifies pulmonary inflammation, and aggravates emphysematous changes in $ApoE^{-/-}$ mice compared with controls, and smoking cessation reverses the inflammatory responses and halts progression of atherosclerosis and emphysematous changes (Boue et al., 2012; Phillips et al., 2015, 2016).

In the present study, we used the $ApoE^{-/-}$ mouse model to investigate the impact of CS or aerosol from two potential MRTPs based on the heat-not-burn principle, CHTP 1.2 and THS 2.2, on the cardiovascular and respiratory system. $ApoE^{-/-}$ mice were exposed to CS from a 3R4F reference cigarette, or to the aerosol from THS 2.2 or CHTP 1.2 (nicotine concentration matched to CS: 28 mg/m^3), over a six-month period. The effects of cessation or switching to CHTP 1.2 aerosol after three months of CS exposure were also investigated. This study complements previous *in vivo* assessment studies for CHTP 1.2 and THS 2.2 (Ansari et al., 2016; Phillips et al., 2018; Smith et al., 2016; Titz et al., 2018). For CHTP 1.2, the current study supports lower effects than 3R4F CS on relevant pathobiological processes, such as atherosclerosis and COPD-related changes; for THS 2.2, this study confirms previous findings on the lower to absent induction of pathobiological processes compared with 3R4F CS in the $ApoE^{-/-}$ mouse model. This study further supports that heating rather that burning tobacco not only reduces the released toxicant yields compared with CS but also consistently induces less pathobiologically relevant effects. More particularly, we observed that in the animal model used in this study the potential MRTPs slow down the progression of CS-induced atherosclerotic and emphysematous changes, suggesting that THS 2.2 and CHTP 1.2 aerosol alone had minimal adverse effects on the cardiovascular and respiratory system. Note that more detailed molecular results will be presented elsewhere.

2. Materials and methods

2.1. General study design

Female $ApoE^{-/-}$ mice were randomized into six groups (Fig. 1): Sham, exposed to filtered air; 3R4F, exposed to CS from the 3R4F reference cigarette (600 µg total particulate matter [TPM]/L aerosol target exposure concentration equivalent to 28 µg nicotine/L); CHTP 1.2, exposed to aerosol from CHTP 1.2 (nicotine levels matched to those of 3R4F CS equivalent to 28 µg nicotine/L); THS 2.2, exposed to aerosol from THS 2.2 (nicotine levels matched to those of 3R4F CS equivalent to 28 µg nicotine/L); Cessation, three months of exposure to 3R4F CS (600 µg TPM/L aerosol) followed by exposure to filtered air; and Switch to CHTP 1.2 aerosol, three months of exposure to 3R4F CS (600 µg TPM/L aerosol) followed by exposure to aerosol from CHTP 1.2 (nicotine levels matched to those of 3R4F CS equivalent to 28 µg nicotine/L). The maximum exposure duration was six months, and interim dissection time points were scheduled after Months 2, 3, 4, and 6, as indicated in Fig. 1. Different dissection groups were dedicated for the different endpoints; see Table 1 for detailed allocation and group sizes.

Table 1
Allocation of mice to groups and endpoint.

Treatment group	Month	BALF	Histopathology	Lung Function	Omics	Micro-CT	Total No. of Mice
Sham	2	10	10	12	10		42
	3	9	10		9		28
	4	9	10		9		28
	6	9	10	3	9	16	47
3R4F	2	10	10	12	10		42
	3	12	12	12	15		51
	4	12	12	12	15		51
	6	12	12	12	15	16	67
CHTP1.2	2	10	10	12	10		42
	3	9	10		9		28
	4	9	10		9		28
	6	9	10	3	9	16	47
THS2.2	2	10	10	12	10		42
	3	9	10		9		28
	4	9	10		9		28
	6	9	10	3	9	16	47
CESS	4	12	12	12	15		51
	6	12	12	12	15	16	67
SWITCH	4	12	12	12	15		51
	6	12	12	12	15	16	67
SUM							882

2.2. Reference cigarettes, potential MRTPs, and test-atmosphere generation

3R4F reference cigarettes were purchased from the University of Kentucky (http://www.ca.uky.edu/refcig). CHTP 1.2 uses a pressed carbon heat source to heat a tobacco plug in a specially designed stick to produce a nicotine-containing aerosol. THS 2.2 consists of a single-use, disposable stick containing a tobacco plug inserted into a holder, containing a battery, electronics for temperature control, a heating element, and the stick extractor (Schaller et al., 2016; Smith et al., 2016), that heats the tobacco electrically in a controlled way to ensure that combustion temperatures are not reached. In both CHTP 1.2 and THS 2.2, the controlled heating of the tobacco generates an aerosol containing mainly water, glycerin, nicotine, and tobacco flavors. For detailed descriptions of CHTP 1.2 and THS 2.2, see (Phillips et al., 2018; Schaller et al., 2016). CHTP 1.2 and THS 2.2 sticks, as well as the holder, were provided by PMI (Neuchâtel, Switzerland).

Mainstream CS from 3R4F cigarettes was generated on 30-port rotary smoking machines as described previously (Phillips et al., 2015), while aerosol from CHTP 1.2 and THS 2.2 sticks was generated on modified 30-port rotary smoking machines equipped with the respective stick holders (Phillips et al., 2016). Two modified smoking machines per chamber were required to achieve the target CHTP 1.2 and THS 2.2 aerosol concentrations. 3R4F cigarettes were smoked, and aerosol from CHTP 1.2 and THS 2.2 sticks was generated, according to the Health Canada Intensive Smoking Protocol (55 ml puff volume, one puff per 30s, and 100% blockage of ventilation holes) (Health Canada, 2000). Several additional minor deviations from this protocol were necessary for technical reasons (Phillips et al., 2015). For example, butt length and static burning rate, typical smoking parameters, were measured only for the 3R4F machines or cigarettes, as they are only relevant for cigarettes. The puff count ranged from 10 to 11 puffs per cigarette (average 10.4 ± 0.3) for the 3R4F sticks. The CHTP 1.2 and THS 2.2 machines were always set for 12 puffs due to device configuration. The 3R4F cigarettes were smoked to a butt length range of 34–36 mm (average 34.6 ± 0.4), and the static burning rate was 467 s per 40 mm.

2.3. Animals and inhalation exposure

All procedures involving animals were performed in an Association for Assessment and Accreditation of Laboratory Animal Care International-accredited, Agri-Food & Veterinary Authority of Singapore-licensed facility with approval from an Institutional Animal Care and Use Committee (IACUC protocol #15015), in compliance with the National Advisory Committee for Laboratory Animal Research Guidelines on the Care and Use of Animals for Scientific Purposes (NACLAR, 2004). Female B6.129P2-Apoe^{tm1Unc} N11 ApoE$^{-/-}$ mice bred under specific pathogen-free conditions were obtained from Taconic Biosciences (Germantown, NY). The mice were approximately six to eight weeks old on arrival and eight to ten weeks old at the start of the exposure. Female mice were chosen due to demonstrated sensitivity to cigarette smoke with respect to development of markers of COPD (Glassberg et al., 2016; March et al., 2006; Tam et al., 2016a; Tam et al., 2016b), and also to align the results with historical data sets (Phillips et al., 2015, 2016). The age and health status of mice on arrival was verified using the health check certificate provided by the breeder. Additional health checks were conducted on live animals (6 animals prior to study start and again at study completion, health screening panel 450M) and serum samples (month 3, health screening panel SM246) (Envigo, U.K).

Mice were kept and exposed under specific hygienic conditions with filtered, conditioned, fresh air at 22 °C ± 2 °C and 55% ± 15% humidity. The light/dark cycle was 12 h/12 h. A maximum of eight mice were housed per cage. Cage enrichment (Igloo™, Biosys Corp. PTE LTD, Singapore, and Nylabone™, Neptune City, NJ) was provided in each cage during the non-exposure period. The bedding material (Lignocel®BK 8–15, J. Rettenmaier & Soehne, GmbH & Co KG., Rosenberg, Germany) was composed of autoclaved softwood (fur and spruce) granulate. A gamma-irradiated pellet diet (T2914C rodent diet, Harlan Laboratories) was provided. For additional details of animal housing, randomization, and acclimatization, see publications on previous studies (Boue et al., 2012, 2013; Phillips et al., 2015, 2016).

A total of 882 mice were allocated to the exposure groups (Table 1) using a randomization sequence stratified by body weight (Provantis, Instem, U.K.). Group allocation was completed four days prior to the exposure start to obtain similar mean body weights for all groups at first exposure day. Group sizes were based on a previously proven statistical design (Boue et al., 2012, 2013; Phillips et al., 2015, 2016) to maintain statistical power and keep low numbers of animals.

The mice were whole-body exposed to diluted mainstream smoke from 3R4F cigarettes (target concentration 600 μg TPM/L, equivalent to 28 μg nicotine/L), CHTP 1.2 aerosol (nicotine-matched to 3R4F, 28 μg/L), THS 2.2 aerosol (nicotine-matched to 3R4F, 28 μg/L), or filtered air for 3 h per day, five days per week, for up to six months. Intermittent

Table 2
Biomarker of CS exposure as well as nicotine exposure. A) Carboxyhemoglobin in blood (%).

			Sham	3R4F	CHTP 1.2	THS 2.2	Cessation	Switch CHTP
COHb (Combined)	**%**	**2M**	Mean	Mean	Mean	Mean		
			2.88 (±) 0.05	35.63 (±) 0.94	4.44 (±) 0.09	3.52 (±) 0.08		
					#	#		
				+	+	+		
		4M	Mean	Mean	Mean	Mean	Mean	Mean
			2.95 (±) 0.02	34.59 (±) 1.47	4.29 (±) 0.08	3.84 (±) 0.05	2.9 (±) 0.02	4.13 (±) 0.06
					#	#	#	#
				+	+	+		+
			Sham	3R4F	CHTP 1.2	THS 2.2	Cessation	Switch CHTP
Nicotine	**ng/mL**	**2M**	Mean	Mean	Mean	Mean		
			13.49 (±) 6.76	147.16 (±) 22.28	79.42 (±) 12.92	108.72 (±) 9.69		
					#			
				+	+	+		
		5M	Mean	Mean	Mean	Mean	Mean	Mean
			2.53 (±) 0.72	212.53 (±) 36.5	100.66 (±) 13.57	112.25 (±) 15.21	9.75 (±) 2.46	110.86 (±) 14.92
					#	#	#	#
				+	+	+	+	+
Cotinine	**ng/mL**	**2M**	Mean	Mean	Mean	Mean		
			38.65 (±) 38.54	266.36 (±) 49.99	255.15 (±) 40.67	271.95 (±) 22.04		
				+	+	+		
		5M	Mean	Mean	Mean	Mean	Mean	Mean
			0.16 (±) 0.06	429.17 (±) 87.43	228.45 (±) 18.21	260.73 (±) 21.37	0.72 (±) 0.17	254.35 (±) 21.06
					#		#	#
				+	+	+	+	+

+ $p < 0.05$ significant versus Sham.
#$p < 0.05$ significant versus 3R4F.

daily exposure to fresh, filtered air for 30 min after the first hour of smoke exposure and for 60 min after the second hour of exposure (Fig. 1) was provided to avoid a build-up of excessive carboxyhemoglobin (COHb) concentrations in the 3R4F group. Previous studies using ApoE$^{-/-}$ mice as a model system (Boue et al., 2012, 2013; Phillips et al., 2015, 2016) demonstrated that this exposure regimen and six-month time frame was sufficient to induce symptoms of both emphysema/COPD and CVD in the ApoE$^{-/-}$ mice and was well tolerated. For the Sham group, mice were exposed to filtered air. Food was unavailable during the exposure period, but the mice had constant access to drinking water. Unexposed reserve mice had free access to food and water throughout the experimental period.

The atmosphere in the aerosol exposure chambers was monitored for flow rate, temperature, relative humidity, concentration, and particle size of TPM as well as the concentrations of carbon monoxide (CO), formaldehyde, acetaldehyde, and acrolein as described previously. For a detailed description of the procedures, see (Phillips et al., 2015, 2016).

2.4. Animal-related procedures

The general condition and health of the mice following exposure were monitored throughout the study. This included weekly body weight measurements, as well as daily group and individual observations after exposure. Animals with identified ailments or injuries were tracked daily on a special observations list until they were deemed fit by the study director, in consultation with the attending veterinarian.

2.5. Analysis of biomarkers of CS and nicotine exposure in blood and urine

Blood COHb concentrations were determined twice during the study, at Months 2 and 4 of exposure, as described previously (Phillips et al.,

Table 3
Blood lipoprotein cholesterol. The first value indicates mean of Total cholesterol, Cholesterol HDL, Cholesterol LDL, Cholesterol VLDL, and Cholesterol CM in mg/dL. Second value corresponds to ± SEM, n = 10–12. Statistics describe comparison with Sham or 3R4F exposed animals. $+p < 0.05$ significant versus Sham. $\#p < 0.05$ significant versus 3R4F.

Treatment group	Total cholesterol				Cholesterol HDL				Cholesterol LDL			
	2M	3M	4M	6M	2M	3M	4M	6M	2M	3M	4M	6M
Sham	Mean	Mean	Mean	Mean	Mean	Mean	Mean	Mean	Mean	Mean	Mean	Mean
	374.13 (±) 44.24	401.45 (±) 31.24	399.38 (±) 29.94	409.75 (±) 30.05	17.55 (±) 2	16.59 (±) 1.97	15.6 (±) 2.33	14.83 (±) 2.01	84.95 (±) 10.72	95.48 (±) 9.02	97.56 (±) 5.39	94.93 (±) 12.66
3R4F	Mean	Mean	Mean	Mean	Mean	Mean	Mean	Mean	Mean	Mean	Mean	Mean
	493.21 (±) 64.38	490.69 (±) 47.99	457.84 (±) 22.14	458.34 (±) 54.71	17.39 (±) 1.97	17.36 (±) 2.04	16.47 (±) 1.25	16.08 (±) 1.66	98.26 (±) 7.34	102.06 (±) 7.06	99.72 (±) 4.32	102.05 (±) 9.19
	+	+	+									
CHTP 1.2	Mean	Mean	Mean	Mean	Mean	Mean	Mean	Mean	Mean	Mean	Mean	Mean
	368.51 (±) 32.41	380.75 (±) 49.94	417.23 (±) 73.84	385.61 (±) 59	17.53 (±) 1.97	17.48 (±) 2.17	18.63 (±) 2.16	17.62 (±) 2.14	93.76 (±) 4.46	95.96 (±) 9.44	102.69 (±) 17.13	93.89 (±) 10.73
	#	#										
THS 2.2	Mean	Mean	Mean	Mean	Mean	Mean	Mean	Mean	Mean	Mean	Mean	Mean
	423.52 (±) 35.49	406.34 (±) 20.88	398 (±) 47.93	440.53 (±) 48.78	20.68 (±) 1.54	16.76 (±) 2.71	16.85 (±) 2.4	20.82 (±) 2.34	100.37 (±) 6	96.72 (±) 8.12	97.57 (±) 9.68	108.87 (±) 11.45
		#	#		#			#				
					+			+	+			
Cessation			Mean	Mean			Mean	Mean			Mean	Mean
			384.01 (±) 44.91	394.41 (±) 31.38			17.95 (±) 2.04	17.85 (±) 1.9			100.28 (±) 9.25	103.25 (±) 9.09
			#									
								+				
Switch CHTP			Mean	Mean			Mean	Mean			Mean	Mean
			391.98 (±) 39.95	462.96 (±) 30.38			17.69 (±) 1.91	17.58 (±) 2.15			100.52 (±) 11.13	115.69 (±) 8.18
			#									#
				+								+

Treatment group	Cholesterol VLDL				Cholesterol CM			
	2M	3M	4M	6M	2M	3M	4M	6M
Sham	Mean	Mean	Mean	Mean	Mean	Mean	Mean	Mean
	238.6 (±) 31.11	260 (±) 21.31	260.42 (±) 22.62	266.99 (±) 22.68	33.03 (±) 6.59	29.37 (±) 2.1	25.79 (±) 4.17	32.99 (±) 8.98
3R4F								

(*continued on next page*)

Table 3 (*continued*)

Treatment group	Cholesterol VLDL				Cholesterol CM			
	2M	3M	4M	6M	2M	3M	4M	6M
	Mean	Mean	Mean	Mean	Mean	Mean	Mean	Mean
	321.72 (±) 52.07	324.36 (±) 35.59	306.72 (±) 19.98	301.23 (±) 46.55	55.83 (±) 8.28	46.89 (±) 6.58	34.92 (±) 4.72	38.97 (±) 6.67
CHTP 1.2	+ Mean	+ Mean	+ Mean	Mean	+ Mean	+ Mean	+ Mean	Mean
	226.29 (±) 26.09	241.68 (±) 37.11	271.15 (±) 53.67	249.72 (±) 42.74	30.9 (±) 3.23	25.61 (±) 6	24.74 (±) 6.29	24.37 (±) 6.23
THS 2.2	# Mean	# Mean	Mean	Mean	# Mean	# Mean	# Mean	# Mean
	263.49 (±) 26.25	263.86 (±) 11.81	259.08 (±) 35.58	284.59 (±) 35.57	38.96 (±) 5.86	28.99 (±) 1.72	24.48 (±) 5.06	26.23 (±) 4.34
Cessation		#	# Mean	Mean	#	#	# Mean	# Mean
			243.58 (±) 33.1	249.61 (±) 22.46			22.19 (±) 3.68	23.69 (±) 3.89
			#				#	#
Switch CHTP			Mean	Mean			Mean	+ Mean
			248.63 (±) 27	301.68 (±) 20.53			25.13 (±) 3.46	27.99 (±) 4.63
			#				#	#
				+				

+ p < 0.05 significant versus Sham.
#p < 0.05 significant versus 3R4F.

2015, 2016). Urine collection was performed for a 24-h period, including the three × 1-h exposure period. Plasma levels of nicotine and cotinine (Months 2 and 5) and the following non-nicotine urinary biomarkers of CS exposure indicating uptake of smoke/aerosol constituents were also measured two times (at Months 3 and 6): hydroxypropyl mercapturic acid (HPMA), S-phenylmercapturic acid (SPMA), 2-cyanoethylmercapturic acid (CEMA), 4-(methylnitrosamino)-1-(3-pyridyl)-1-butanol (NNAL). From the same samples urinary biomarkers of oxidative stress and inflammation were measured: 4-hydroxynonenal, malondialdehyde, tetranor-PGE-M, 2,3-dinor-8-iso-prostaglandin F2α ($PGF_{2\alpha}$), 8-iso-$PGF_{2\alpha}$, 2,3-dinor-thromboxane B2 (TXB2), 11-dehydro-TBX2, and 12-hydroxyeicosatetraenoic acid. These biomarkers were determined externally (ABF GmbH, Munich, Germany); for details, see (Supplementary Table 1) and (Phillips et al., 2015, 2016).

2.6. Lung function measurements and lung volume determination

Lung function measurements (Supplementary Table 2) were made in anaesthetized, tracheotomized, and cannulated mice using the flexiVent™ rodent ventilator system for measurement of respiratory mechanics (SCIREQ, Montreal, Canada), as described previously (Phillips et al., 2015, 2016). Lung volume of the lungs that were scheduled for histopathology was determined by displacement of fixative under hydrostatic pressure (15 cm H_2O) (Scherle, 1970).

2.7. Hematology and clinical chemistry

Blood samples were drawn from mice under terminal pentobarbital anesthesia from the retro-orbital venous plexus, and blood platelets, erythrocytes, hematocrit, and hemoglobin counts and levels were analyzed using a Sysmex XT-2000i analyzer (Sysmex Corp., Kobe, Japan) as described previously (Phillips et al., 2015, 2016). Serum lipid profiles and triglyceride, lipoprotein, cholesterol as well as cholesterol chylomicron levels were determined by external company (LipoSEARCH, Skylight Biotech, Akita, Japan) (Table 3; Supplementary Table 3).

2.8. Dissection

Dissections were performed after Months 2, 3, 4, and 6 of exposure. At each dissection time point, animals were allocated to the following endpoints: bronchoalveolar lavage fluid (BALF), including analysis of infiltrated inflammatory cells in lungs and multi-analyte (cytokines/chemokines) profiling of BALF; histopathological evaluation and morphometry of lungs; lung function; and plaque surface area determination (aortic arch, planimetry), and plaque surface area and volume determination (aortic arch and thoracic aorta, Micro CT). Molecular analysis (transcriptomics, proteomics, miRNA, genomics) were performed after Months 3, 4, and 6 of exposure (Fig. 1). Following the analysis of the molecular results obtained from month 3, 4, and 6, further analysing the month 2 tissue samples collected for downstream molecular analysis was discontinued as it was deemed unlikely to provide additional information above the month 3 samples results (Omics dissection group, Table 1).

2.9. Bronchoalveolar lavage analysis

BALF was obtained from nine to 12 mice per group (Table 1), and the number and classification of free lung cells (FLC) (flow cytometry) as well as the concentrations of inflammatory mediators (Luminex-based multi-analyte profiling using Rodent Map 3.0) were measured (Fig. 9**)**. Gelatin proteolytic activity (EnzChek® Gelatinase/Collagenase Assay Kit; Life Technologies (Invitrogen), Singapore) was determined as described previously (Phillips et al., 2015, 2016). Additional BALF samples were sent to Ampersand Biosciences (https://www.ampersandbio.com/) to assess the concentrations of inflammatory mediators (Supplementary Table 4**)**.

2.10. Histopathology

Lungs were fixed by instillation with ethanol glycerol acetic acid formaldehyde solution (4% formaldehyde, pH 7.4) at a fixed pressure (15 cm H_2O) and processed as described previously (Boue et al., 2013). The left lung lobe was serially sectioned (4 μm thick) in approximately 20 step sections (150 μm apart) for an overall assessment of the entire lung lobe. Representative paraffin and/or cryosections were also obtained from the nose and lung tissue. The sections were stained with hematoxylin and eosin (H&E) and Alcian blue periodic acid-Schiff reagent for the left lung and nose (polysaccharides and glycoproteins, including mucus) and resorcin-fuchsin for the left lung (elastic fibers). Histopathological evaluation of the left lung (serial sections) and nose (three predefined levels imaging the respiratory nasal epithelium (RNE), the olfactory epithelium, the olfactory bulb, and the molar teeth) was performed in a blinded fashion by a board-certified veterinary pathologist as described previously (Boue et al., 2013; Kogel et al., 2014; Phillips et al., 2015; Stinn et al., 2010). Semi-quantitative severity grading in five steps was performed for each finding.

Digitalized (Aperio slide scanner) serial sections of the lung were also evaluated for alveolar emphysema (semi-quantitative scoring and quantitative morphometry (Supplementary Table 5). Morphometry was performed using a design-based stereological approach to obtain quantitative data (newCAST™, Visiopharm, Hoersholm, Denmark) addressing the characteristics of alveolar emphysema (i.e., tissue destruction and hyperinflation) by different endpoints (for details, see (Phillips et al., 2015, 2016). Semi-quantitative histopathological evaluation and quantitative lung morphometry were carried out by a board-certified veterinary pathologist in a blinded fashion (Histovia GmbH, Overath, Germany).

2.11. Plaque size measurements

After removal of the aortic arch, the aortic arch wall was opened longitudinally and stained with Oil Red O, and the intimal area covered by plaques normalized to the whole area was determined from digital images using a Visiopharm image analysis module (for details, see (Boue et al., 2012; Lietz et al., 2013)). For an independent, complementary measurement, the aortic arch and thoracic aorta plaque segment were measured with micro-CT scanning at Month 6. Sixteen mice per group were grossly dissected (trimming of ribs and removal of forelimbs, GI tract, and liver) and placed into neutral-buffered formalin (4% v/v) fixative and sent to Scanco Medical AG (Brüttisellen, Switzerland) for micro-CT imaging and measurement of plaque volume and plaque surface.

2.12. Tissue processing for systems toxicology and omics analyses

Tissues for molecular analysis were collected at Months 3, 4, and 6 of exposure. Tissues were collected 16–24 h after exposure (separate samples from the same tissues/organs for transcriptomics, proteomics, lipidomics, and genomics) from six to nine mice per group (For transcriptomics analysis 7-9 mice per group (Line 240) were used. RNE n = 8–9, heart ventricle n = 9, lung n = 8–9, aorta n = 7–9. miRNA lung n = 7–9. For proteomics analysis in lung n = 6–8 mice were used. For DNA methylation analysis in Lung n = 8–9. Mice dedicated for molecular analysis were selected from OMICS group (Table 1) and processed as described previously (Phillips et al., 2016).

2.12.1. Gene and miRNA expression analysis

Total RNA was isolated from tissues using the miRNeasy Mini Kit

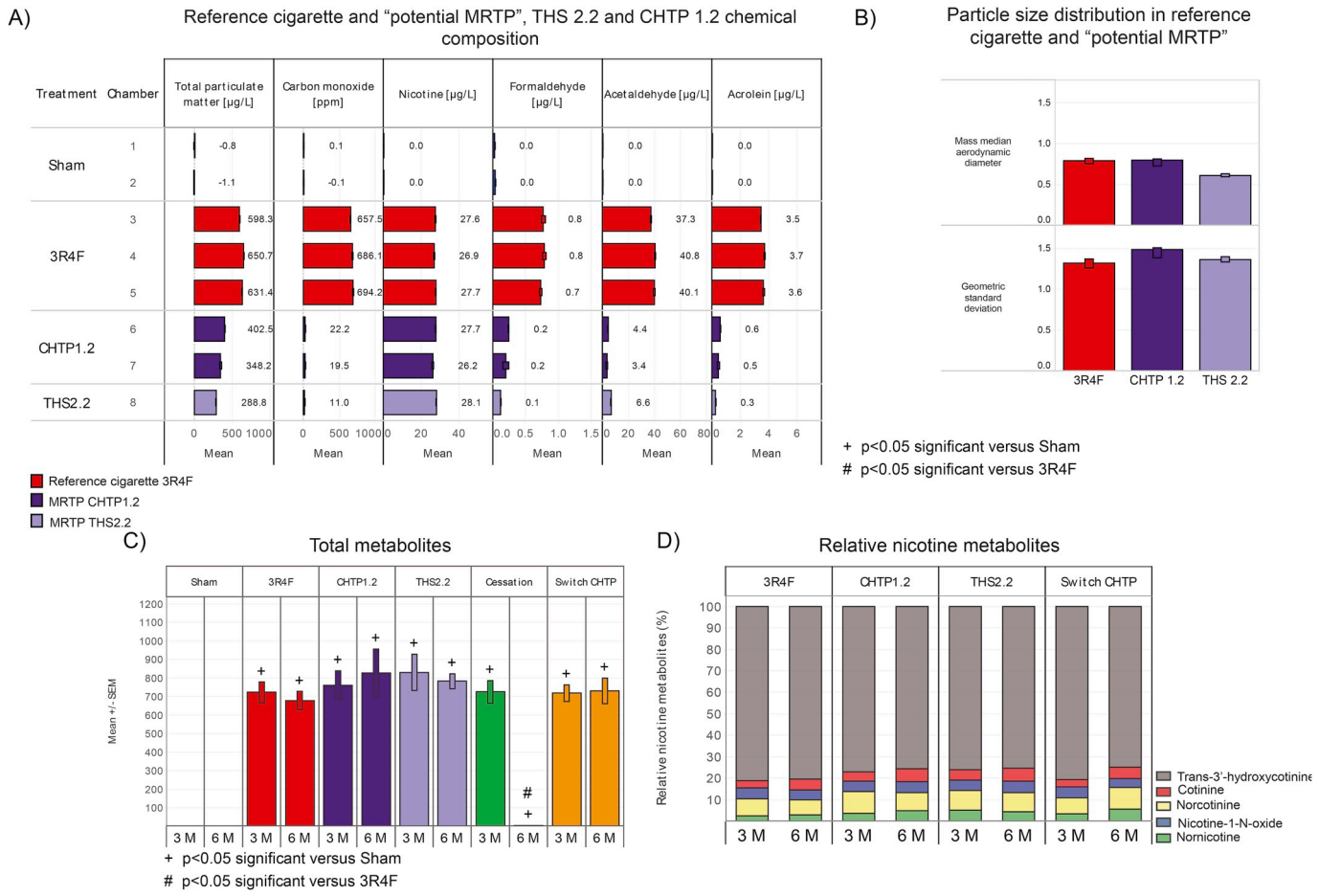

Fig. 2. Test atmosphere exposure and nicotine biomarkers. (A–B) Test atmosphere characterization in 3R4F CS and "potential MRTP" THS 2.2 and CHTP 1.2. Data are shown as Mean ± SD. (C) Nicotine metabolites in urine. Relative level of five nicotine metabolites: trans-3′-Hydroxycotinine, cotinine, norcotinine, nicotine, nicotine-1′-N-oxide, nornicotine. (D) Absolute level of total metabolites in urine in nmol. Data are means ± SEM, n = 11–21.

(Qiagen, Hilden, Germany) and quality-checked using an Agilent 2100 Bioanalyzer (Agilent Technologies, Santa Clara, CA, USA). Total RNA (100 ng) was reverse-transcribed, amplified, purified, and hybridized on MG430 2.0 GeneChips (Affymetrix, Santa Clara, CA, USA) and evaluated using standard procedures (Phillips et al., 2015, 2016). miRNA was analyzed using microarrays and a previously described method (Zanetti et al., 2017). (Data have been deposited in the ArrayExpress database under accession number E-MTAB-7444).

Transcriptomic data on the lung were analyzed in the context of hierarchically structured network models describing the molecular mechanisms underlying essential biological processes in non-diseased lungs (Boue et al., 2015; Hoeng et al., 2012). Leveraging the "cause-and-effect" network models together with network perturbation amplitude (NPA) algorithms, the gene expression fold-changes were translated into differential values for each network node (Martin et al., 2012, 2014). These were in turn summarized into a quantitative NPA measure, and NPA values were aggregated into a biological impact factor (BIF); details have been described elsewhere (Kogel et al., 2014; Phillips et al., 2015).

2.12.2. Proteomics procedures

Our general quantitative proteomics approach has been reported previously (Phillips et al., 2015), and specific details are given in Phillips et al. and Ansari et al. (Ansari et al., 2016; Phillips et al., 2016). The mass spectrometry proteomics data have been deposited into the database of the ProteomeXchange Consortium (Vizcaino et al., 2014) via the PRIDE partner repository with the dataset identifier PXD010875 (Lung), PXD010873 (Heart).

2.13. DNA methylation assessment by whole-genome bisulfite sequencing

2.13.1. DNA extraction, bisulfite conversion, and sequencing

Genomic DNA was extracted from tissues using the QIAamp tissue mini kit (QIAGEN). One hundred nanograms of genomic DNA and 0.5 ng of unmethylated lambda DNA (Promega, Madison, WI, USA) were re-suspended in 52.5 µL Tris-EDTA buffer. The DNA was sheared using a Covaris E220 sonicator (Woburn, MA, USA) to obtain double-strand DNA (dsDNA) fragments of approximately 200 bp. After ligation of indexed sequencing adapters from the Ovation Ultralow Methyl-Seq Library System (NuGEN Technologies, San Carlos, CA, USA), bisulfite conversion was carried out using the EpiTect Bisulfite Kit (QIAGEN). The converted dsDNA was recovered using a MinElute PCR Purification Kit (QIAGEN), amplified by PCR, and cleaned on Agencourt RNAClean XP beads (Beckman Coulter, Brea, CA, USA). The concentrations and sizes of the sequencing libraries were verified on a bioanalyzer (Agilent). Normalized libraries were pooled in multiplexes of 6–14 libraries and clustered on Illumina PE high output flow cell v3 using an Illumina cBot and Illumina TruSeq PE Cluster Kit v3-cBot-HS kits (Illumina, San Diego, CA, USA). Sequencing was performed on an Illumina HiSeq 2500 or HiSeq 4000 system using Illumina TruSeq SBS v3-HS kits (200 cycles) and Illumina TruSeq PE Cluster Kit v3-cBot-HS in a 2 × 101 paired-end mode.

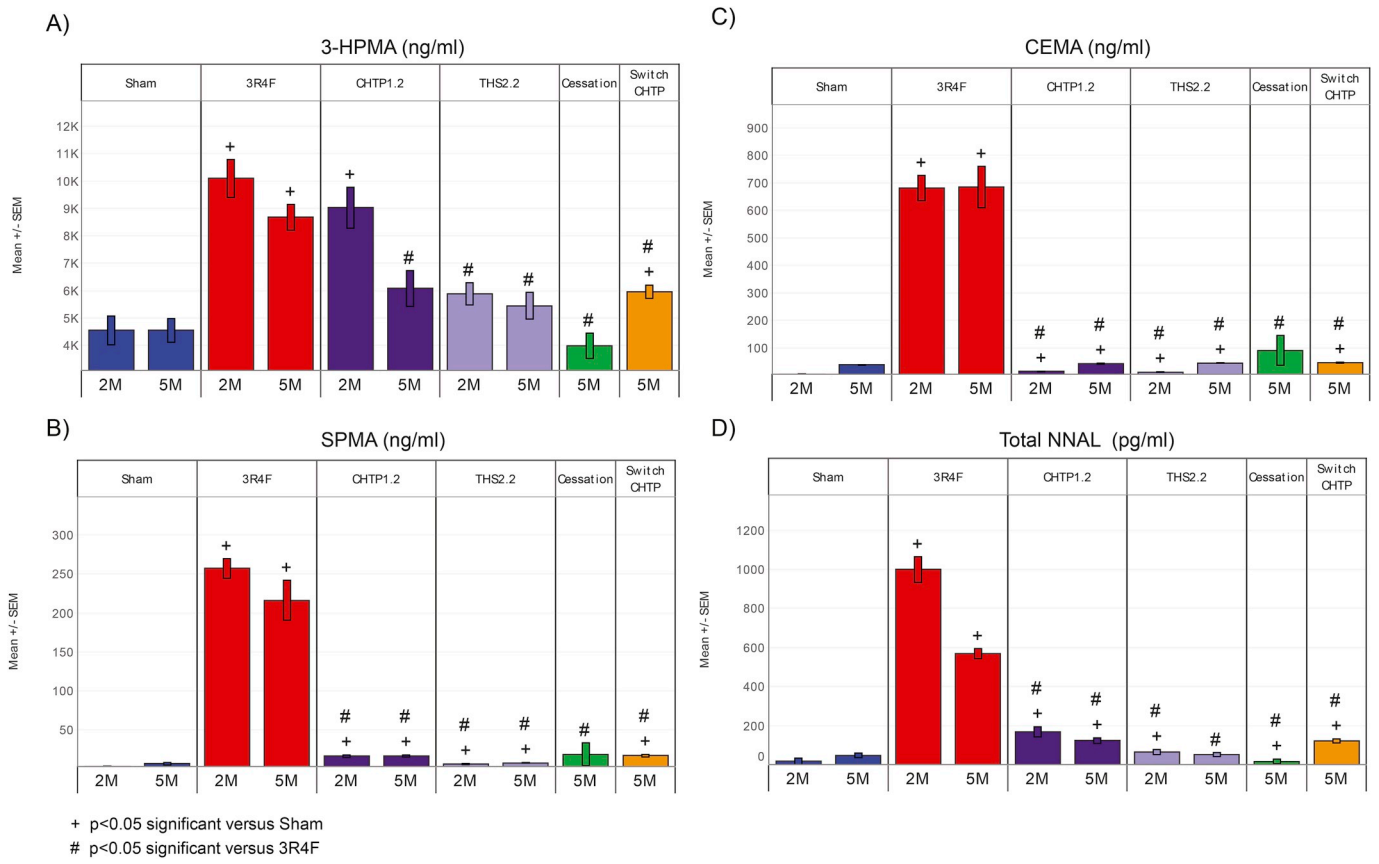

Fig. 3. Biomarkers of CS exposure in urine. (A) 3-HPMA. (B) SPMA. (C) CEMA. (D) Total NNAL. Data are means ± SEM, n = 10–13.

2.13.2. Data processing

Sequencing reads were aligned to the mouse genome (version mm10) using the qAlign function in the QuasR package (v. 1.10.0) (Gaidatzis et al., 2015) which uses bowtie (v. 1.10.0) internally with alignment parameters fitting directional bisulfite-converted libraries. Methylation was quantified using the qMeth function from the QuasR package. Only cytosines in a CpG context were considered, and the counts were strand-combined.

2.13.3. Identification of low-methylated regions (LMRs) and unmethylated regions (UMRs)

Mammalian methylomes can be segmented into three main classes: fully methylated regions (FMR), unmethylated regions (UMR), and low methylated regions (LMR). FMRs present 90% of the genome, UMRs correspond to CpG islands and active promoters, and LMRs correspond to enhancers (Stadler et al., 2011). Therefore, DNA methylation signal can be used to identify regulatory elements. In the current study, LMRs and UMRs were identified using methylSeekR package (Burger et al., 2013) with default parameters and without partially methylated domain filtering. LMRs were detected for every experimental group by merging the counts for the respective replicates. LMRs from all experimental conditions were combined into one unified set. To reduce locus redundancy, LMRs with more than 60% overlap were merged, leading to a collection of 121,260 loci (Supplementary Figure 1). This unified set was used in all subsequent analyses. Methylation levels for all the elements in the unified set of LMRs were quantified separately for every replicate and used to compute differential methylation between the treatment samples and the respective Sham control samples. To ensure the accuracy of LMR detection and the role of these regions as potential enhancers, we took advantage of the public ChIP-seq (chromatin immunoprecipitation sequencing) data performed from lung and liver chromatin of eight-week-old mice (GEO: GSE29184) (Shen et al., 2012). We quantified monomethylation of histone H3 at lysine 4 (H3K4me1), trimethylation of histone H3 at lysine 4 (H3K4me3), and acetylation of histone H3 at lysine 27 (H3K27ac) histone marks and the input control (DNA extracted from the chromatin prior to the immunoprecipitation) at LMRs and UMRs detected in Sham-exposed mice at the Month 3 time point. As expected, LMRs harbored an enhancer signature, which consists of high H3K4me1 and H3K27ac and low H3K4me3 signals. By contrast, UMRs were enriched in H3K4me3 and H3K27ac signals, which are hallmarks of active promoters, and showed a low level of H3K4me1 signal (Supplementary Figure 1).

2.13.4. Identification of differentially methylated loci

Differential methylation was computed for regulatory elements that are promoters and candidate enhancers. Promoters were defined as non-overlapping −500-bp to +500-bp intervals around transcription start sites from the RefSeq database. (https://www.ncbi.nlm.nih.gov/refseq/). Candidate enhancers were defined as LMRs. Read counts were summed per region, and methylation levels corresponding to the ratio between methylated and total events were presented on a 0–1 range, with 0 representing a fully unmethylated state (methylated counts = 0) and 1 representing a fully methylated state (methylated counts = total counts). The significance of differential methylation between the treatment groups and the respective controls was assessed using the false discovery rate (FDR)-adjusted *p*-value from the beta-binomial model implemented in the *betabin* function from the aod package (https://cran.r-project.org/web/packages/aod/index.html). The coupled values (number of methylated counts and number of unmethylated counts) per replicate were used as input. For each contrast (treatment vs. control), only loci covered by at least 15 reads in all the computed samples were considered. The methylation difference between

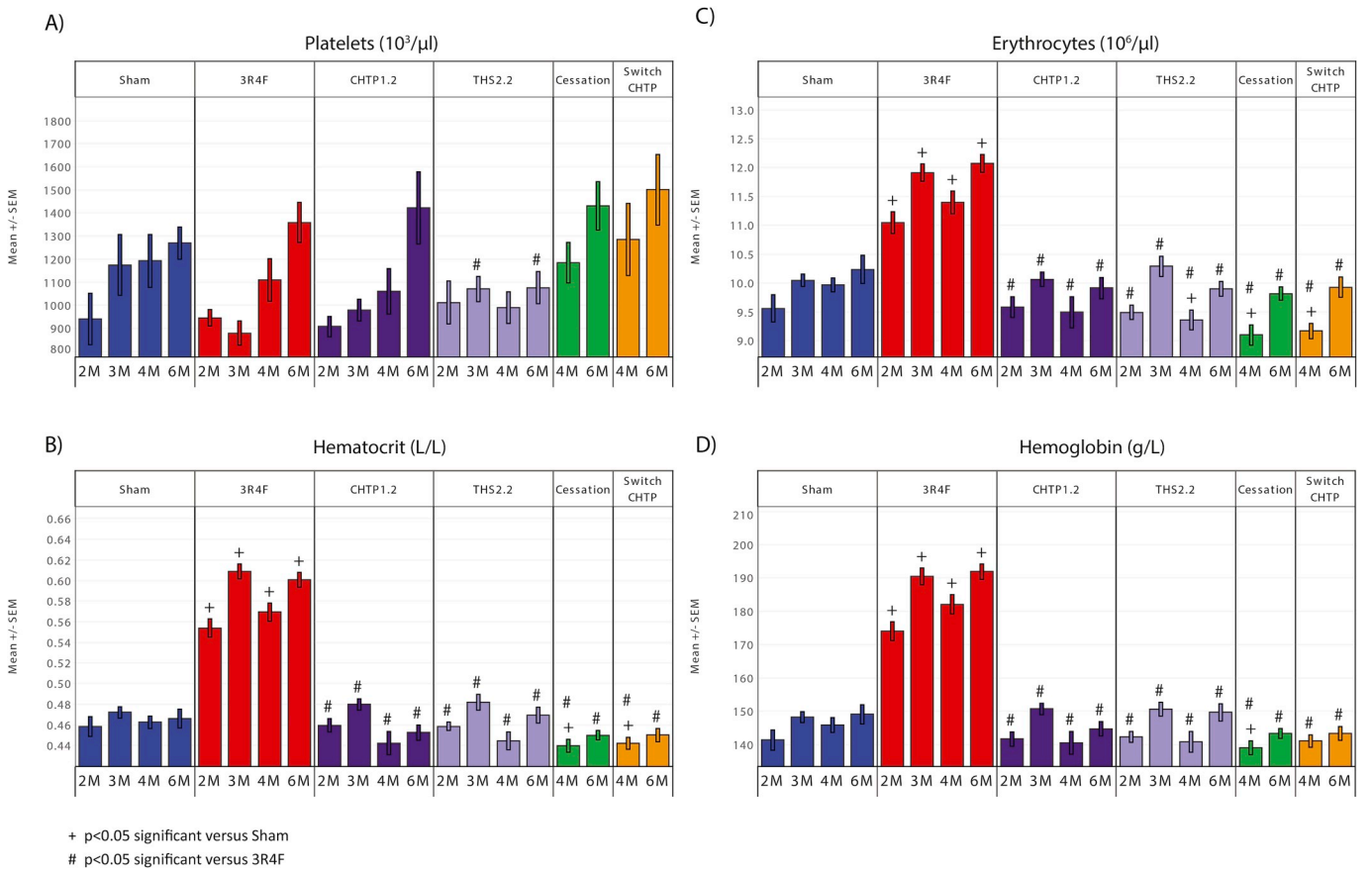

Fig. 4. Hematology. (A) Platelets, (B) Erythrocytes, (C) Hematocrit, and (D) Hemoglobin were counted or measured in blood. Platelets and erythrocytes were reported as relative number of cells per µl (number/µl). Data are means ± SEM, n = 9–12.

treatment and control was calculated as follows: the sum of methylated reads in treatment group divided by the sum of total reads in treatment group minus the sum of methylated reads in control group divided by the sum of total reads in control group.

2.14. Statistical analysis

Unless otherwise indicated, data are expressed as means ± standard error of the mean (SEM). Pairwise comparisons between groups were performed, and unadjusted *p*-values are stated. For continuous variables, if the data of the two groups being compared did not exhibit strong deviation from the normal distribution (as assessed by performing a Shapiro-Wilk test at the 5% level on the standardized residuals of both groups), a two-sample *t*-test accounting for variance heterogeneity was performed. Otherwise, an exact Mann-Whitney-Wilcoxon two-sample test was used (to save computing time, Monte Carlo estimates of the exact *p*-values were used). For body weight comparisons, and because the sample size per group was greater than 30, only the *t*-test was performed. For score variables (histopathology), the Cochran-Mantel-Haenszel test was used, and the Fisher exact test was used for incidence variables. All analyses were performed with the SAS system 9.2. Results were considered to be significantly different in a specific comparison if $p < 0.05$.

2.15. Data availability

Datasets and additional data visualizations can be accessed at: https://www.intervals.science/studies/#/Apoe-CHTP12-THS22.

3. Results

3.1. Aerosols generated from potential MRTPs contain lower levels of carbon monoxide, TPM, and HPHCs than 3R4F CS

CS from 3R4F cigarettes and aerosols from CHTP 1.2 and THS 2.2 were generated, diluted, and delivered to the exposure chambers. Aerosol target concentrations in the exposure chambers were set at 28.0 µg nicotine/L (equivalent to 600 µg TPM/L from conventional 3R4F CS) for all test and reference item groups (3R4F, CHTP 1.2 and THS 2.2 exposure groups). Average nicotine concentrations across all chambers ranged from 27.5 to 27.7 µg/L for the 3R4F chambers, ranged from 26.1 to 27.7 µg/L for the CHTP 1.2 chambers, and averaged 28.1 µg/L for the THS 2.2 exposure chamber, which were all within the specified study target range of ± 10% of target concentrations (Fig. 2A) and were maintained during the 6-month exposure period (Supplementary Table 1). Carbon monoxide concentrations in the CHTP 1.2 and THS 2.2 test atmospheres were 96% and 98% lower than for the 3R4F group. The levels of the harmful and potentially harmful constituents (HPHC) acetaldehyde, acrolein, and formaldehyde were approximately 83–89%, 85–95% and 69–83% lower, respectively, in CHTP 1.2 and THS 2.2 aerosols compared with 3R4F CS (Fig. 2A). Of note, whereas the composition of TPM between the potential MRTPs and CS is different and cannot be directly compared (Schaller et al., 2016), we observed that the TPM concentration in the CHTP 1.2 and THS 2.2 test atmosphere was 40% and 53% lower, respectively, than in the 3R4F test atmosphere.

The particle size distribution was measured per chamber on a monthly basis during the study, and the resulting mass median aerodynamic diameter (MMAD) and geometric standard deviation (GSD)

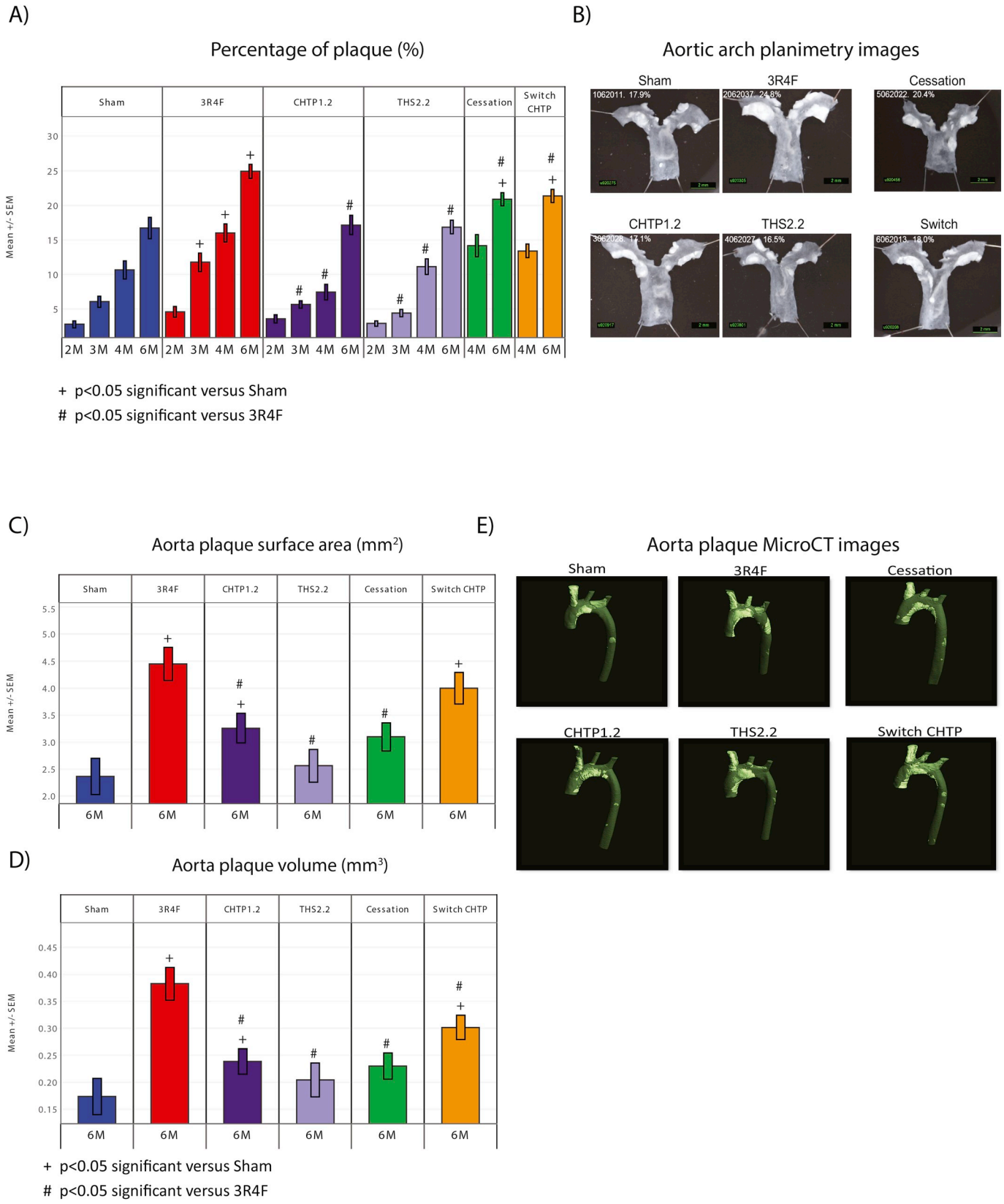

Fig. 5. Atherosclerotic plaque area measurements. (A–B) Aortic arches were dissected and opened longitudinally for planimetry analysis. Atherosclerotic lesion area as well as aortic arch area were measured at Months 2, 3, 4, and 6 of exposure. Atherosclerotic plaque area was divided by total aortic arch area to represent plaque progression in percent. (A) Percentage of plaque area. (B) Planimetry pictures representing plaque area in aortic arch at Month 6 of exposure. Data are means ± SEM, n = 17–27. (C-D-E) Atherosclerotic plaque progression measured with micro-CT based on aortic arch and thoracic aorta segment was performed at Month 6 of exposure. Atherosclerotic plaque surface and volume were identified in aorta and measured. (C) Plaque surface area reported in mm^2. (D) Plaque volume reported in mm^3. (E) CT scan images, the highlighted part of the aorta represents atherosclerotic lesions. Data are represented as absolute value means ± SEM, n = 16.

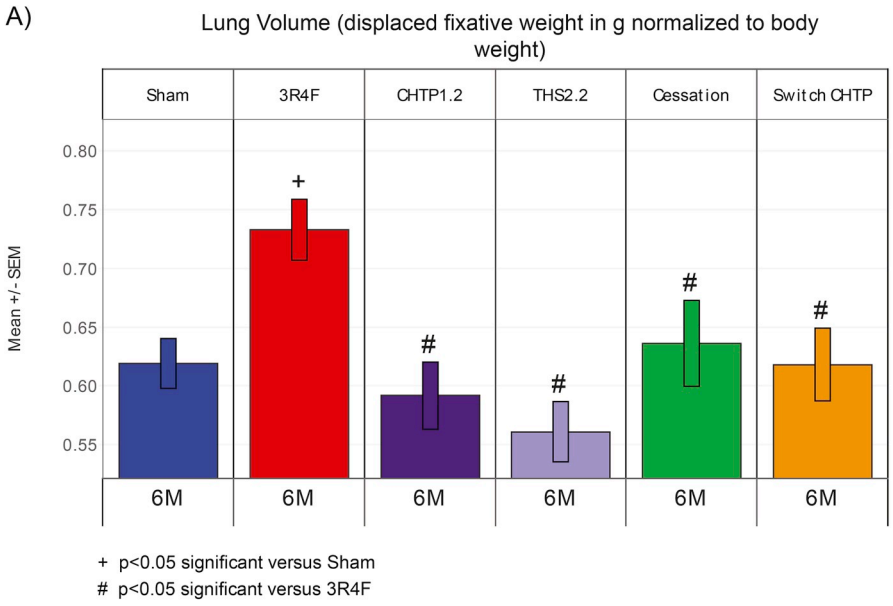

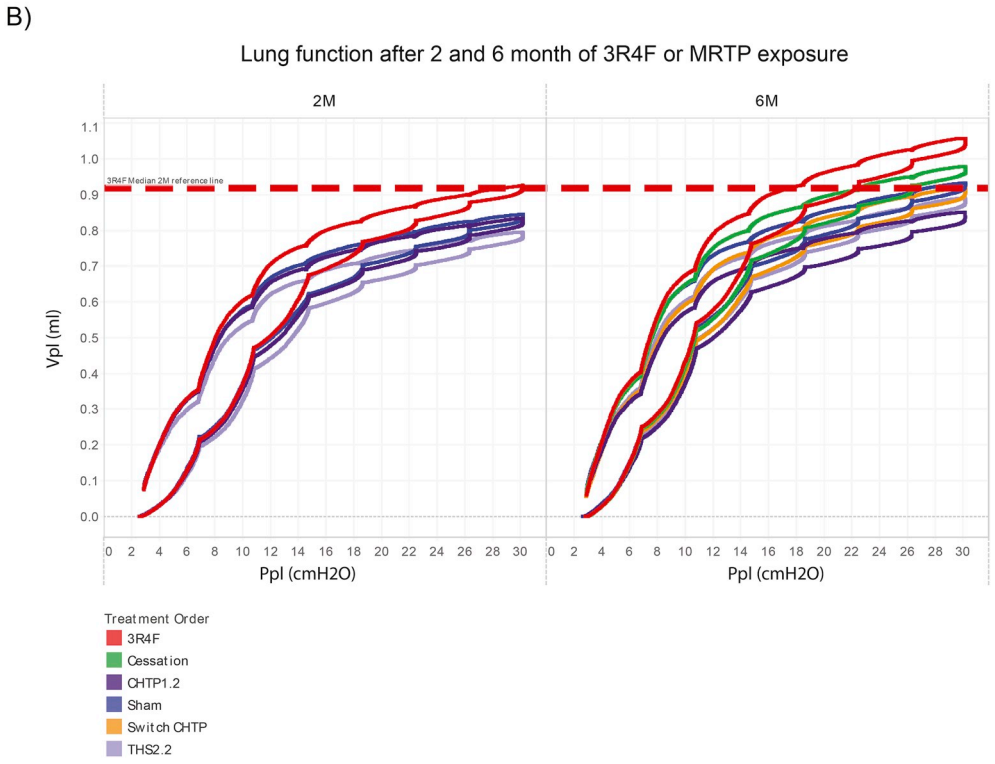

Fig. 6. Lung volume and function after exposure to 3R4F CS or MRTP aerosol. Lungs were removed, and volumes were determined by displacement of fixative under hydrostatic pressure. (A) The plots represent the relative volume related to body weight in grams at Month 6. Mean ± SEM, n = 10–12. (B) Pressure/volume loops at Months 2 and 6 of exposure. Lung function was measured in selected animals 18–24 h after exposure using the SCIREQ flexiVent™ system. "Airway" constriction and lung "stiffness" were assessed by measuring pressure, flow, and volume relationships in the respiratory system and by using forced oscillations to discriminate between airway and lung tissue variables according to complex mathematical models (for details, see Phillips et al., 2015). The relationship between pressure (Ppl, pressure plethysmography) and the resultant volume (Vpl, volume plethysmography) over an inflation/deflation cycle is shown. Data are median without SDs, n = 9–10.

values for 3R4F, CHTP 1.2, and THS 2.2 chambers were analyzed. The MMAD and GSD ranged from 0.78 to 0.79 µm and 1.27–1.35, respectively, for the 3R4F chambers, from 0.75 to 0.85 µm and 1.43–1.57, respectively, for the CHTP 1.2 chambers, and 0.61 µm and 1.36, respectively, for the THS 2.2 chamber (Fig. 2B). Consequently, and based on similar particle sizes and distributions, the deposition in the lungs in of mice exposed to CS from 3R4F or to aerosols from THS 2.2 and CHTP 1.2 would be expected to be similar.

3.2. Biomonitoring demonstrates uptake of potential MRTP aerosol and 3R4F CS

Blood COHb levels were analyzed two times in the study, at Months 2 and 4 of exposure (Table 2A). As expected, the percentages of COHb in the blood samples were consistently considerably higher in the 3R4F-exposed group (average 34–35% for Months 2 and 4, respectively), compared with the fresh air-exposed group. The test atmospheres from CHTP 1.2 and THS 2.2 aerosols nicotine-matched to 3R4F had considerably lower CO contents (Phillips et al., 2018; Schaller et al., 2016) due to the low CO deliveries of the products, which was reflected by the lower blood COHb levels detected in the animals of the chronically exposed THS 2.2 and CHTP 1.2 and Switch groups in the Month 4 sampling period (where concentration averaged 3.5–4.5% COHb, respectively). The Cess group had COHb levels similar to those measured in Sham group animals (Cess 2.9% COHb and Sham 2.8% COHb).

Post-exposure plasma samples revealed that the nicotine and

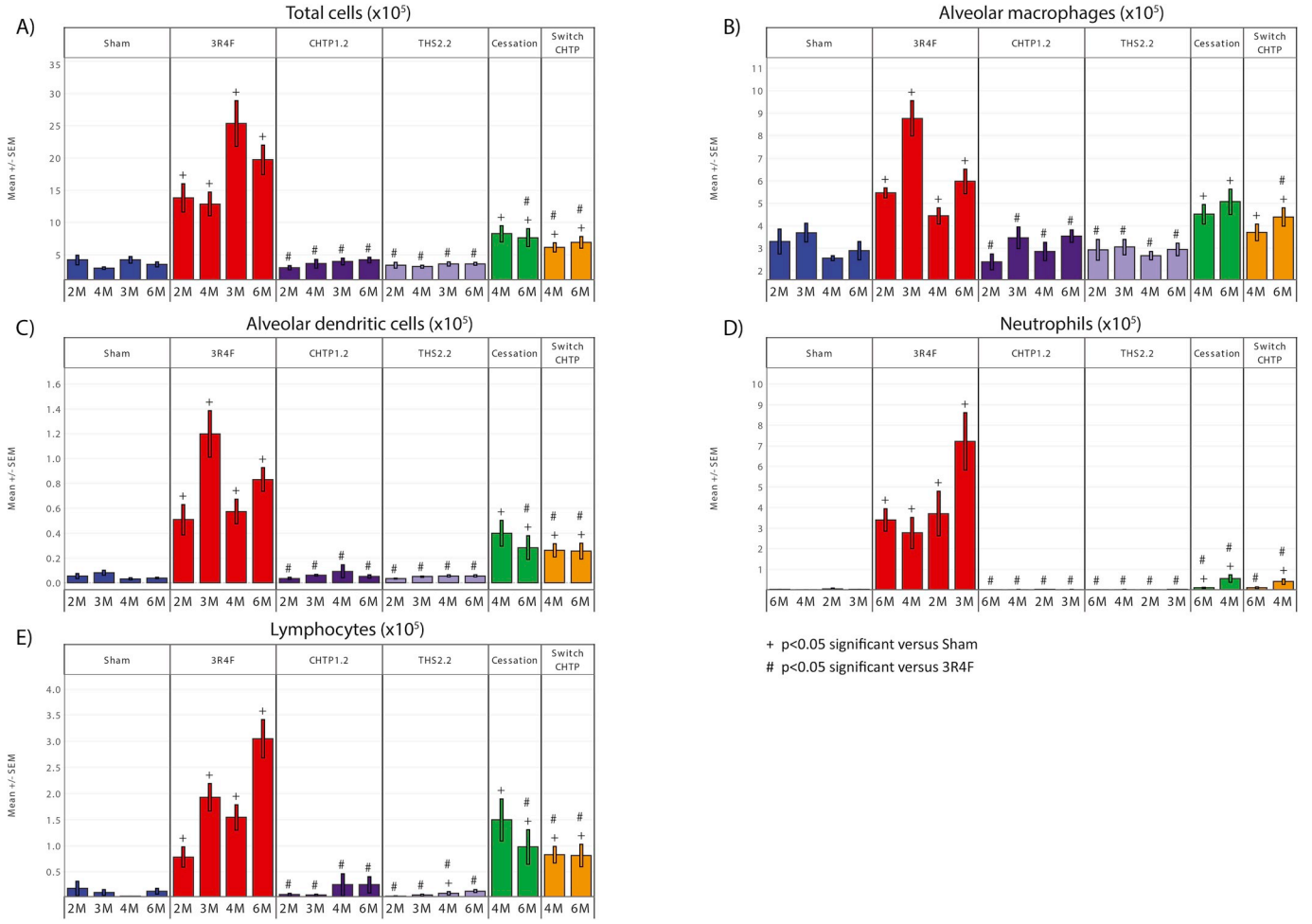

Fig. 7. Inflammatory cells in BALF. Number and subtype of inflammatory cells in BALF were measured by flow cytometry. Data are represented as absolute number of inflammatory cells. (A) Total inflammatory cell number. (B) Alveolar macrophages count. (C) Alveolar dendritic cells count. D) Neutrophils count. E) Lymphocytes count. Data are means ± SEM, n = 9–12.

cotinine concentration (Months 2 and 5) were higher in the 3R4F-exposed animals as well as CHTP 1.2- and THS 2.2-exposed mice (Table 2B) compared with the Sham-exposed mice. Surprisingly, higher nicotine and cotinine concentrations (+47–52% nicotine and +53–60% cotinine) were found in the 3R4F-exposed animals relative to the CHTP 1.2- and THS 2.2-exposed mice at Month 5 of exposure (Table 2B). Both nicotine and cotinine were detected at very low levels (but above the lower limit of quantification) in the Sham-exposed and cessation groups (Table 2B). This may reflect a slight contamination of samples during collection or analysis. However, examination of the chamber concentrations as well as total and relative nicotine metabolites (cotinine, nicotine, nicotine-1′-N-oxide, norcotinine, nornicotine, trans-3′-Hydroxycotinine) from urine showed that the relative nicotine concentrations and total nicotine metabolites (Months 3 and 6) were consistent and closely comparable between potential MRTP- and CS-exposed groups (Fig. 2C and D).

Additionally, urinary biomarkers of exposure to HPHCs were measured. SPMA, CEMA, and Total NNAL were significantly reduced in CHTP 1.2 and THS 2.2 as well as in the Cess and Switch groups compared with the 3R4F group, indicating that the internal exposure to HPHCs was reduced in mice exposed to aerosol from potential MRTPs, consistent with the lower HPHC yields generated by these products (Fig. 3B, C, D). The 3-HPMA level (reflecting exposure to exogenous acrolein as well as metabolism of endogenous acrolein (Zheng et al., 2013), was significantly increased following exposure to 3R4F CS and – only at Month 2 - CHTP 1.2 aerosol. 3-HPMA levels also present significant reductions in comparison with 3R4F CS at Months 2 and 5 of exposure to THS 2.2 aerosol and at Month 5 in the CHTP 1.2, Cess, and Switch groups, in the latter at a level that is statistically significantly higher than in the Sham group but does not exceed the level seen for continuous CHTP 1.2 aerosol exposure (Fig. 3A).

3.3. Potential MRTPs aerosol decreases the impact from CS exposure on erythrocyte counts, hematocrit and hemoglobin content in blood

Erythrocyte counts, hematocrit, and hemoglobin levels were higher in animals exposed to 3R4F CS than in sham-exposed animals, while no significant changes were observed in response to MRTP (CHTP1.2 or THS2.2) aerosol exposure (Fig. 4B–D). Similarly, three months after cessation or switching to CHTP 1.2, a return to normal (Sham-exposed) levels for these parameters (Fig. 4B–D) was achieved. Note that an impact of 3R4F CS exposure on hematocrit and hemoglobin was also observed in a previous seven-month inhalation study with C57BL/6 wt and ApoE$^{-/-}$ mice (Phillips et al., 2015, 2016). We did not observe any significant effect on blood platelets in response to CS or aerosols from either of the potential MRTPs, compared with Sham-exposure (Fig. 4A).

3.4. CS exposure reduces body weight gain in ApoE$^{-/-}$ mice

Body weights increased throughout the study in all groups (Supplementary Figure 2). The Sham-exposed animals had a typical body weight gain profile, reaching an average weight of 29.3 g at the

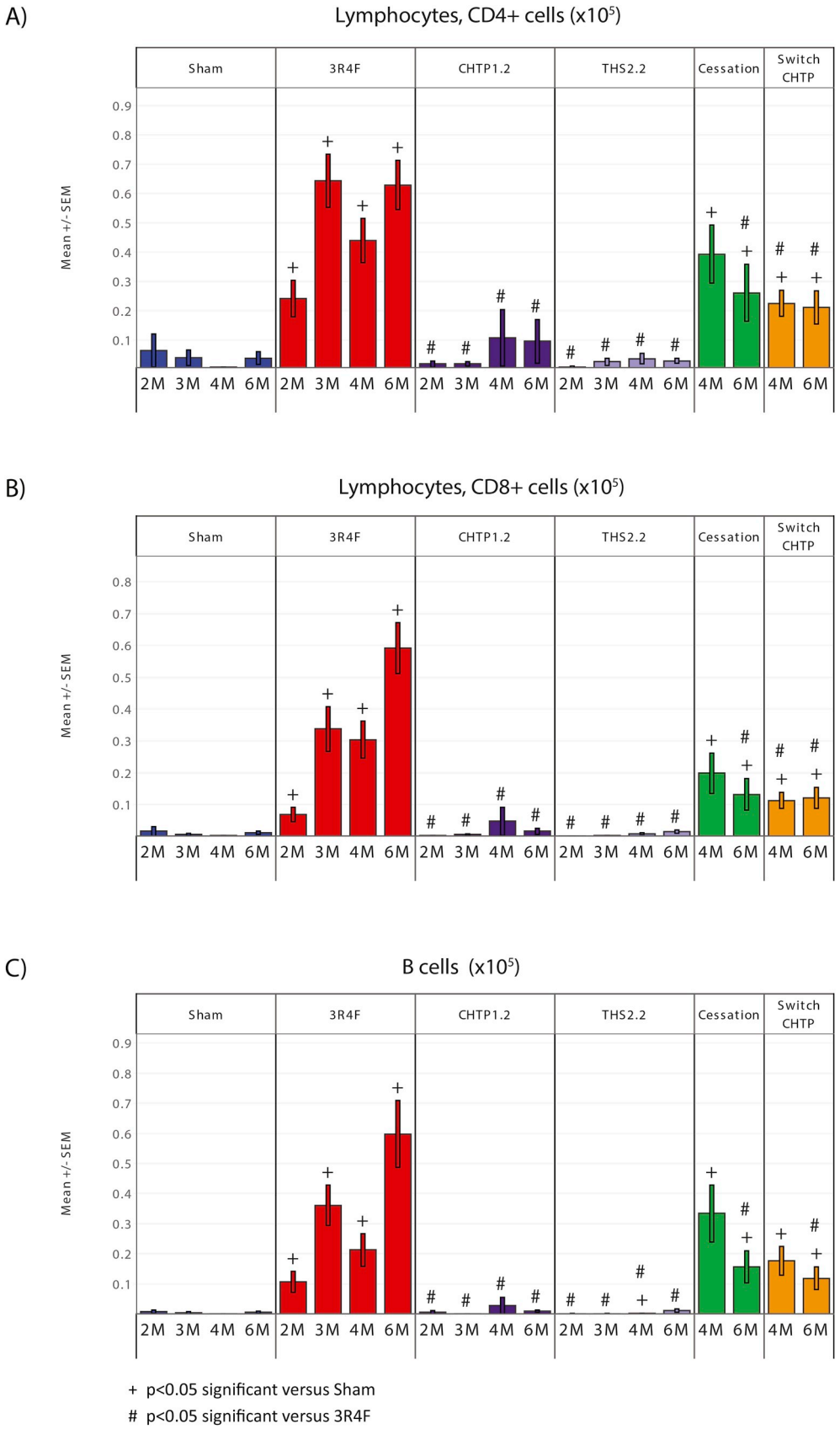

Fig. 8. Inflammatory lymphocytes in BALF. Subtypes of inflammatory lymphocytes in BALF were measured by flow cytometry. Data are represented as absolute number of inflammatory cells. (A) Lymphocytes, $CD4^+$ cells. (B) Lymphocytes, $CD8^+$ cells. (C) B cells. Data are means ± SEM, n = 9–12.

Name	3R4F			CHTP1.2			THS2.2			Cessation		Switch CHTP	
	3M	4M	6M	3M	4M	6M	3M	4M	6M	4M	6M	4M	6M
CXCL1 (Cxcl1)	8.22 +++	11.81 +++	4.75 +++	0.92	1.20	0.50	0.82	1.58	0.88	5.85 +++	1.38	4.44 +	2.15
CXCL10 (Cxcl10)	3.83 +++	6.39 +++	2.77 +++	1.08	1.40	0.55	0.86	1.65 +++	0.64	2.21 +++	1.04	1.85 +++	0.89
INTLK5 (Il5)	1.48	2.88 +	1.22	1.39	1.10	0.20	0.96	1.72	0.46	2.31	0.51	1.90	0.49
INTLK6 (Il6)	4.04 +++	6.97 +++	2.15	4.02	1.78	0.14	2.02	1.64	0.41	3.54 +	0.41	3.14	0.47
INTLK17 (Il17a)	3.31	1.65	2.01 +	0.77	0.77	0.44	0.71	1.57	0.49	3.51	0.43	1.03	0.53
MCP1 (Ccl2)	12.27 +++	11.32 +++	12.00 +++	1.20	1.01	0.66	1.23	1.04	0.74	1.43	1.11	1.47	1.27
MIP1A (Ccl3)	2.03 +++	2.67 +++	2.66 +++	1.04	1.00	0.63	0.82	0.98	0.82	0.67	0.69	1.03	0.78
MIP1B (Ccl4)	14.93 +++	14.66 +++	20.16 +++	1.00	1.00	1.00	1.00	1.00	1.00	1.54	1.39	1.57	1.98
MMP9 (Mmp9)	33.10 +++	36.19 +++	14.34 +++	1.00	0.92	0.35	0.98	1.36	0.58	8.09 +	1.79	6.75 +	2.73
PAI1 (Serpine1)	2.98 +++	3.84 +++	3.00 +++	0.92	1.46	1.02	1.10	1.53 +	0.92	1.86 +++	1.30	1.63 +	1.08
TNF (Tnf)	2.66 +++	2.48 +++	2.47 +	1.00	0.98	0.76	1.08	1.01	0.82	1.35	0.98	1.42	0.99

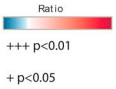

Fig. 9. Inflammatory mediators in BALF. Cell-free BALF supernatants were analyzed using a multiplexed bead array. Ratio is given as median of treated mice over median of Sham-exposed mice at the same time point (truncated scale). Analytes with statistically significant differences compared with Sham are highlighted with + $p < 0.05$, + + + $p < 0.01$, n = 9–12. Red color indicates significantly upregulated analytes, blue color indicates significantly downregulated analytes. Analytes with significant correlation between the presented Milipore analysis and an independent analysis conducted by Ampersand are reported (Supplementary Fig. 4); the heatmap for analytes with low level of correlation is reported in Supplementary Fig. 5.

end of the study. Weight gain was lower in 3R4F CS-exposed mice, with the body weights becoming significantly different from those of Sham-exposed animals after Month 2 of exposure ($p < 0.05$). The body weight profiles of animals chronically exposed to THS 2.2 or CHTP 1.2 aerosol were both trending slightly higher than those of Sham-exposed animals (not significant), consistent with a similar trend observed in previous (Phillips et al., 2015, 2016). Following cessation or switching to CHTP 1.2, the exposed mice gained weight rapidly, approaching (but not quite reaching) the Sham group body weight by the end of the exposure period. Overall, the effects of exposure to 3R4F CS or MRTP aerosols were similar to what had been observed in previous studies (Phillips et al., 2015).

3.5. Cardiovascular parameters

3.5.1. 3R4F CS exposure increases levels of cholesterol and low-density lipoprotein (LDL) and very low-density lipoprotein (VLDL) cholesterol in plasma

The results indicated an increase in total cholesterol, low-density lipoprotein (LDL) cholesterol, and very low-density lipoprotein (VLDL) cholesterol in the 3R4F CS-exposed group ($p < 0.05$) relative to Sham-exposed mice (Table 3) in Month 2 through Month 4. Exposure to CHTP 1.2 had no significant effect relative to Sham on LDL cholesterol, VLDL cholesterol, and total cholesterol. However, THS 2.2 exposure was associated with higher high-density lipoprotein (HDL) cholesterol levels at Months 2 and 6 of exposure and a higher LDL cholesterol level observed only at Month 2 of exposure (Table 3). Mice that were switched from 3R4F CS to CHTP 1.2 aerosol had higher total cholesterol, LDL cholesterol, and VLDL cholesterol compared with the Sham, with levels approaching or exceeding that of 3R4F CS-exposed mice by Month 6 (Table 3).

3.5.2. Potential MRTPs aerosol exposure results in reduced development of atherosclerotic plaques in ApoE$^{-/-}$ mice

Image analysis measurements of the plaque area in the aortic arch revealed the expected increase of relative plaque size (plaque area) for this ApoE$^{-/-}$ mouse model, indicating atherosclerosis progression in all groups over the six-month exposure period (Fig. 5A and B). From Month 3 onward, a significantly increased aortic plaque area was observed in mice exposed to 3R4F CS compared with either Sham-exposed mice or with mice exposed to CHTP 1.2 or THS 2.2 aerosols. Exposure to CHTP 1.2 or THS 2.2 aerosols resulted in similar plaque area sizes compared with Sham-exposed animals ($p > 0.05$ across all time points). Both cessation and switching to CHTP 1.2 groups showed relatively similar plaque area measurements, which were between Sham and 3R4F group levels at Month 4 (indicating a diminished progression) and were significantly different from both the Sham and the 3R4F groups at Month 6 (Fig. 5A and B).

These results were supported using micro-CT imaging of the thoracic aorta in a separate cohort of mice (Fig. 5C–E). 3R4F-exposed mice presented an increase of plaque volume and plaque surface area after six months of exposure in comparison with Sham-exposed mice (Fig. 5CD). CHTP 1.2 and THS 2.2, cessation, and switching to CHTP 1.2 groups had significantly lower plaque surface area and volume in comparison with 3R4F; however, a slight increase of plaque volume and surface area compared with Sham group values was observed in the CHTP 1.2 and switching to CHTP 1.2 groups at Month 6 (Fig. 5C–E). Overall, atherosclerotic plaque evaluation *in situ* by micro-CT imaging at Month 6 confirmed the planimetric results at the aortic arch for 3R4F exposure (Fig. 5B and E).

3.6. Respiratory parameters

3.6.1. Effect of CS and potential MRTPs exposure on lung volume and function

The lung volume (as a measurement of displaced fixative weight) of the 3R4F CS group was higher than that in the Sham, CHTP 1.2, or THS 2.2 groups (Fig. 6A). This was observed consistently throughout all dissection time points. After three months of cessation or switching to CHTP 1.2, the lung volumes reached similar levels observed in Sham-exposed animals.

Since the majority of the "Quick Prime-3, Constant-phase model" and "Negative pressure forced expiration" methods listed in Supplementary Table 2 did not show any significant or persistent (over time) treatment effects (data not shown), the analysis is focused only on the PVsP relationship. The pressure-volume relationship (PVs-P)

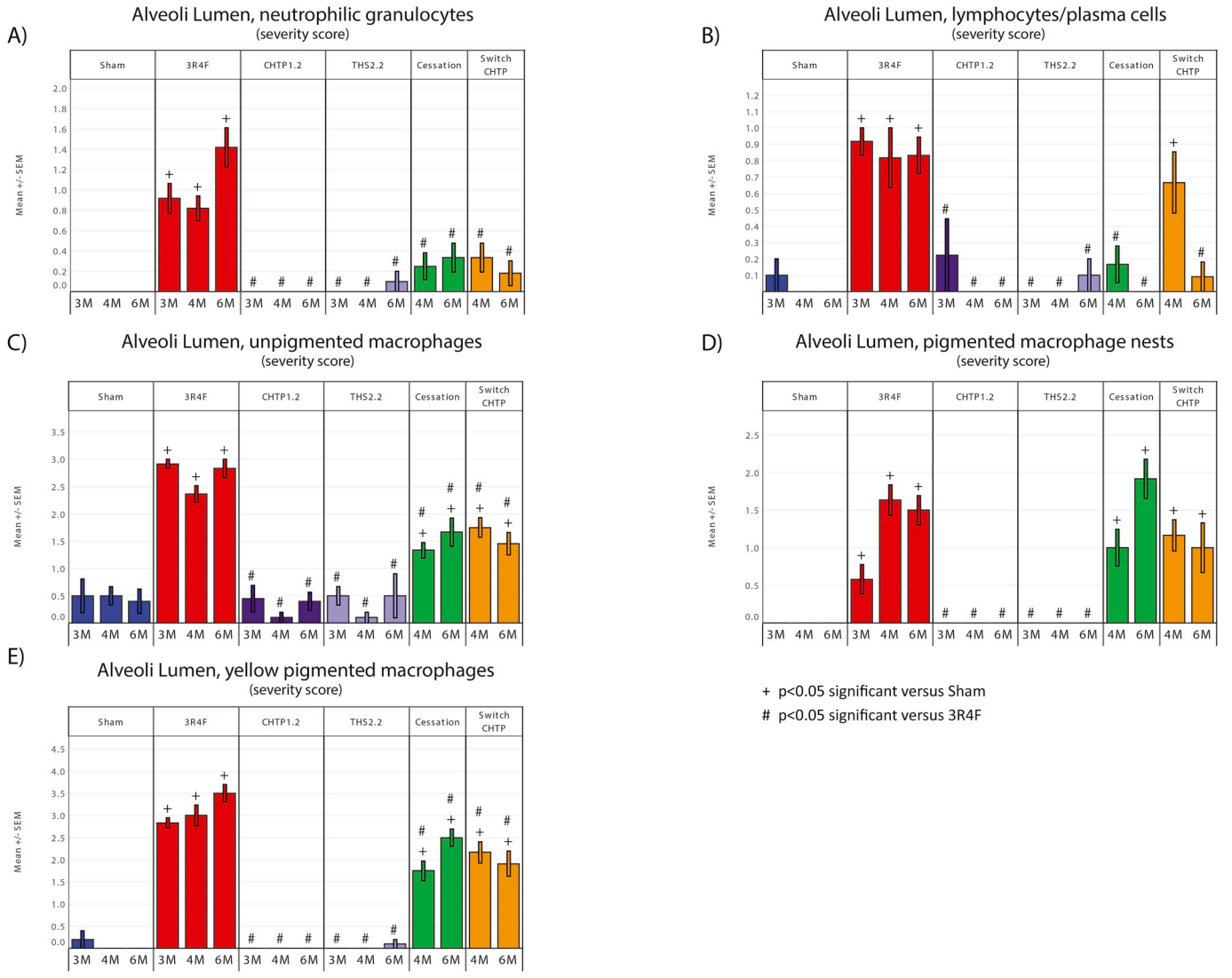

Fig. 10. Histopathological evaluation of inflammatory cell infiltration in the alveolar lumen. Lung tissue was sectioned and stained with H&E, and the abundance of inflammatory cells and type were evaluated with a scoring method (0–5 score). Histograms represent the mean score for (A) Alveolar lumen, neutrophilic granulocytes. (B) Alveolar lumen, lymphocytes/plasma cells. (C) Alveolar lumen, unpigmented macrophages. (D) Alveolar lumen, pigmented macrophage nests. (E) Alveolar lumen, yellow pigmented macrophage. Data are means ± SEM, n = 9–12.

demonstrated a typical emphysema-like upward/leftward shift in the PVs-P loop in the CS-exposed mice as compared with that from the Sham-exposed animals, indicative of CS-induced emphysematous changes in the lung at six months (Fig. 6B). There was no obvious effect of THS 2.2 aerosol exposure on the PVs-P loop compared with the Sham-exposed mice at any of the time points evaluated (Supplementary Figure 3). Switching and cessation resulted in stabilization of the values, while continued 3R4F exposure led to further increases in the PVs-P values. The increased lung volume seen in the CS-exposed mice supports the lung function results, whereby CS exposure resulted in a leftward shift in the PVs-P loop.

3.6.2. Potential MRTPs aerosol exposure results in lower inflammatory cell influx into the lung than 3R4F CS exposure

As expected, the total number of inflammatory free lung cells in the BALF was higher in 3R4F CS-exposed mice than in the Sham- or potential MRTP-exposed groups (Fig. 7A). Similar changes were also seen in the inflammatory cell sub-populations: 3R4F CS-exposed mice demonstrated an increase in the numbers of neutrophils, macrophages, lymphocytes, and dendritic cells (Fig. 7B–E). The strongest 3R4F CS exposure-related change was observed for neutrophils, followed by lymphocytes, dendritic cells, and macrophages, a consistent effect on the differential FLC counts as compared with previous CS inhalation studies (Phillips et al., 2015, 2016, 2018). In contrast to the CS effect on FLCs, even prolonged exposure to either the CHTP 1.2 or the THS 2.2 aerosol had no significant effect on FLC levels, either absolute or differential counts relative to Sham exposure. Both cessation and switching resulted in lower total FLCs in the BALF, even one month after the intervention, though the levels did not change further after an additional two months of exposure (fresh air or CHTP 1.2), suggesting an initial rapid but partial reduction of the inflammatory cell infiltrations.

Following exposure to fresh air or to either of the potential MRTP aerosols (CHTP 1.2 or THS 2.2), very few lymphocytes were present in the BALF (Fig. 7E). In response to 3R4F CS exposure, elevated lymphocyte numbers were observed, as represented by an increased absolute number of $CD4^+$ and $CD8^+$ lymphocytes and B cells (Fig. 8). At most time points following CS exposure, each of the lymphocytic subsets were increased relative to Sham. Switching and cessation resulted in a decreased relative level of $CD4^+$ and $CD8^+$ lymphocytes as well as B cells, though not yet reaching the low lymphocyte numbers of the Sham-exposed group, even after three months of switching/cessation.

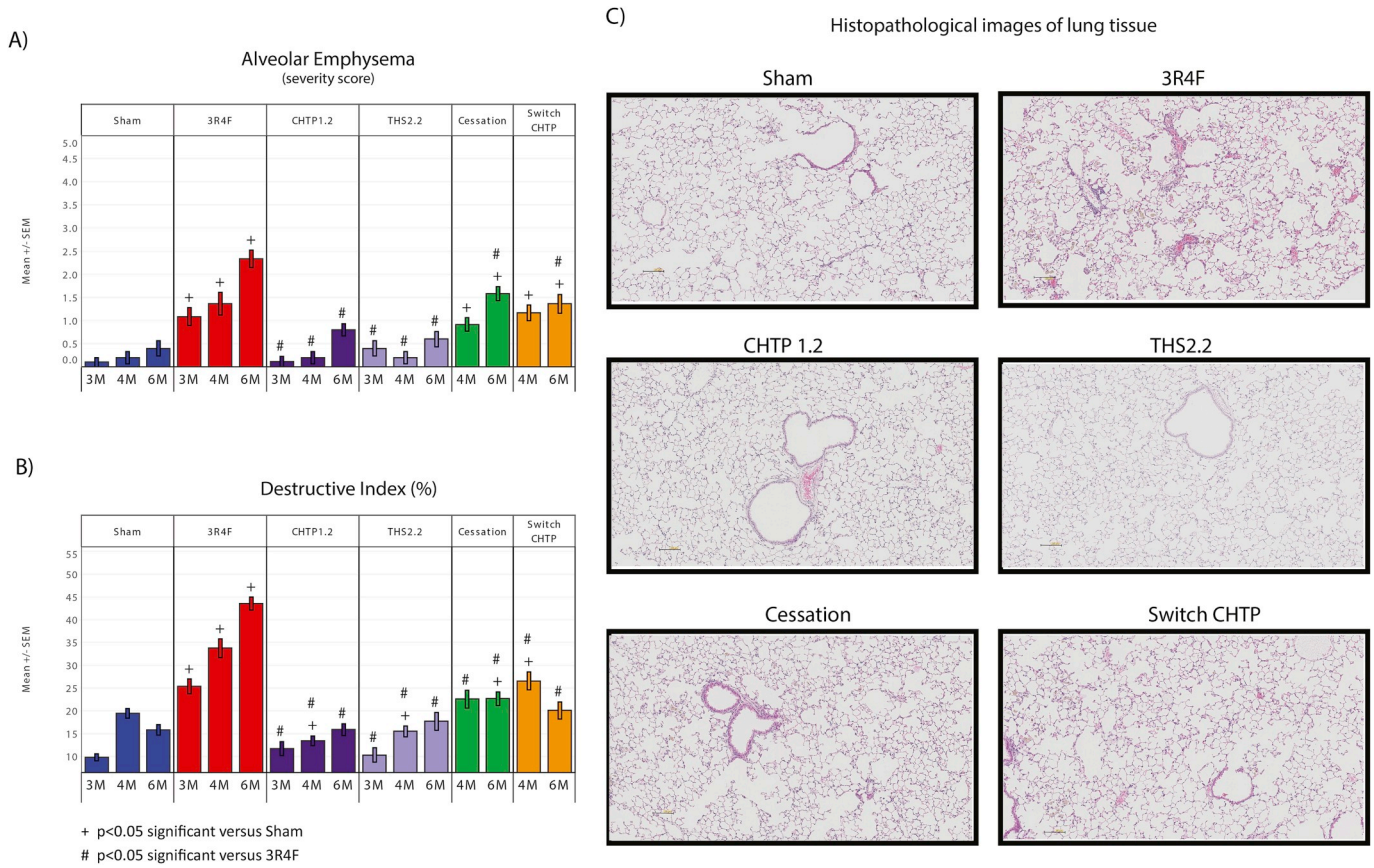

Fig. 11. Histopathological and morphological evaluation of emphysema in lung tissue. (A) Alveolar emphysema (severity score 1–5 scale). (B) Destructive index (%). (C) Histological images of lung tissue representative of emphysematous changes. 20X Image magnification. Data are means ± SEM, n = 9–12.

The lymphocyte subsets were nonetheless significantly lower ($p < 0.05$) than the continuous 3R4F-exposed group by Month 6 (Fig. 8).

3.6.3. 3R4F CS exposure exerts a higher impact on pro-inflammatory mediator levels in BALF than exposure to MRTPs aerosols

Following 3R4F CS exposure, a significant increase in the abundance of inflammatory mediators in the BALF was observed (Fig. 9) as early as Month 3 of exposure, consistent with the increased number of inflammatory FLCs. Chronic exposure to CHTP 1.2 (six months) had only a minimal effect on inflammatory mediators in the BALF. Chronic THS 2.2 exposure showed only two analytes that differed significantly from Sham-exposed mice at Month 4 of exposure, CXCL10 (chemokine (C-X-C motif) ligand 10) and PAI1 (Serine (or cysteine) peptidase inhibitor, clade E, member 1), though the levels were still considerably lower than those seen in the 3R4F-exposed mice. Cessation and switching resulted in a return to Sham exposure levels for most of the cytokines and chemokines analyzed (Fig. 9). No significantly dysregulated mediators were observed in the Switch group at Month 6. In response to 3R4F CS exposure, analytes that showed exposure-related changes were mainly proteins associated with extracellular matrix (ECM) and ECM remodeling (MMP9), and inflammation such as inflammatory chemokine (C-C motif) ligand 2 (CCL2), CCL3, CCL4, CXCL10, CXCL1, IL17A, and TNF. These findings are therefore aligned with the influx of inflammatory cells also detected in the BALF as well as the effects of smoke on the pulmonary ECM as associated with the progression of emphysematous changes (Arunachalam et al., 2010; Li et al., 2017). Overall, these results are consistent with previous BALF analyses in animals exposed to CS or aerosols from the potential MRTPs (Phillips et al., 2015).

3.6.4. Potential MRTPs aerosol exposure results in decreased inflammatory cell infiltration in lung tissue

Histopathological evaluation further confirmed that inflammatory infiltration in the lung was mainly restricted to the 3R4F CS group: increased numbers of neutrophils, lymphocytes, and macrophages were observed in the alveolar spaces of CS-exposed mice from Month 3 onward (Fig. 10). No significant differences to the Sham group were seen in these parameters following exposure to CHTP 1.2 and THS 2.2 aerosols at all time-points. Decreases but not total elimination of the inflammatory infiltrates were observed in the Switch and Cess groups in comparison with 3R4F CS-exposed animals, particularly for macrophage cells, indicating only partial recovery during the subsequent three months (Fig. 10). This is consistent with previous observations in CS-exposed A/J mice that had persistent pigmented macrophage nests even after 13 months of cessation following a 5-month CS exposure period (Stinn et al., 2013).

3.6.5. Potential MRTPs aerosol exposure results in decreased lung injury and lower emphysematous scores

Histopathological semi-quantitative scoring of alveolar emphysema (Fig. 11A, and representative images shown in Fig. 11C) showed significantly increased severity in 3R4F-exposed mice compared with Sham-exposed mice from Month 3 onward, with a progressive increase documented over time. No significant differences for alveolar emphysema were seen from CHTP 1.2 and THS 2.2 aerosol-exposed mice relative to Sham-exposed mice. Both cessation and switching to CHTP 1.2 slowed or stopped the progression of emphysema development seen as alveolar emphysema score, resulting in significantly lower scores compared with 3R4F CS exposure at the month 6 dissection time-point. Of note, switching or cessation did not improve the morphological signs of emphysema beyond the 3-month level, and the scores at the 6-month

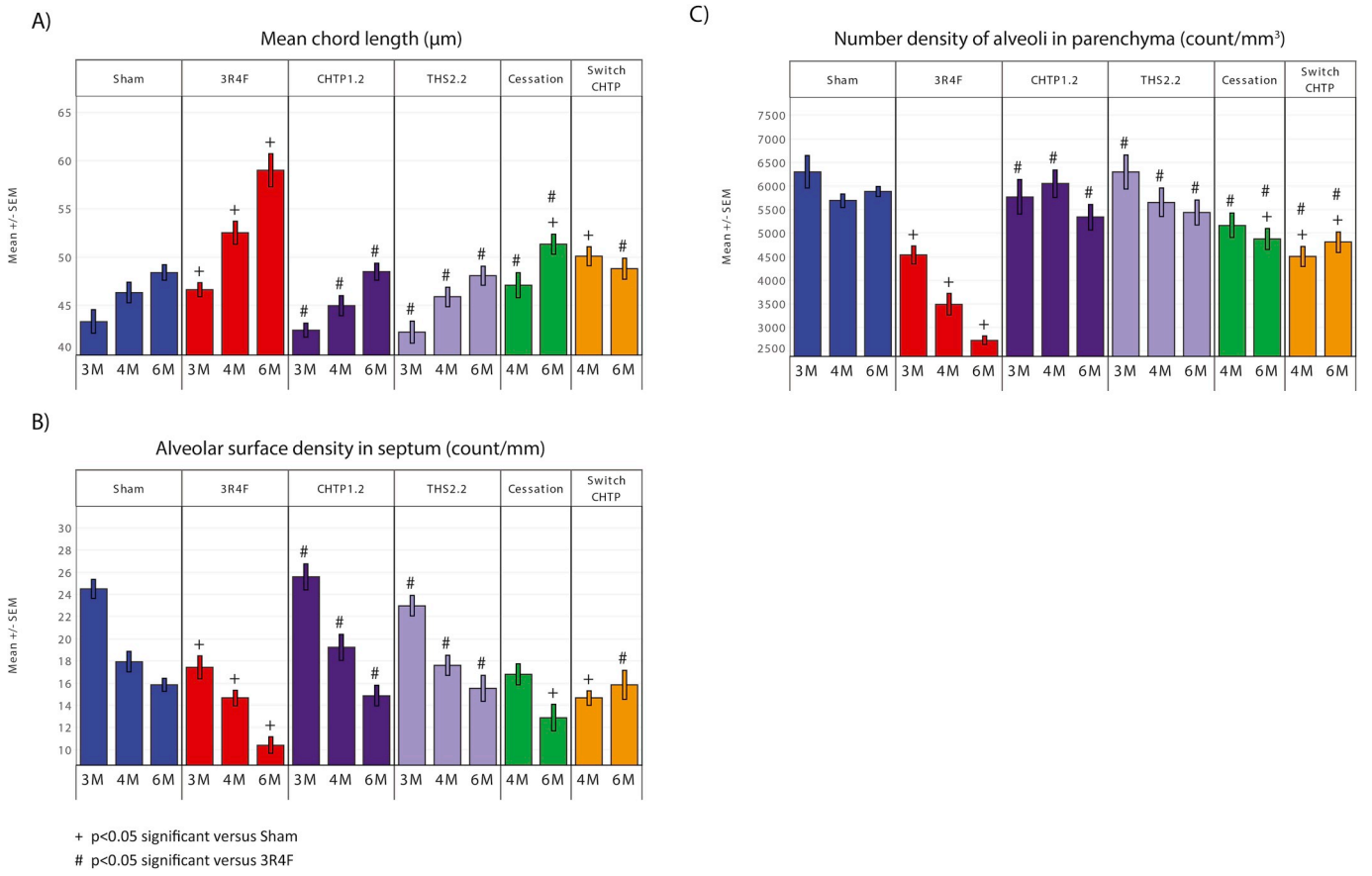

Fig. 12. Morphometric evaluation of lung tissue. (A) Mean chord length (μm). (B) Number density of alveoli in parenchyma (count/mm^3). (C) Alveolar surface density in septum (count/mm). Data are means ± SEM, n = 9–12.

time-point were still higher than those in the Sham group. These histopathological findings were confirmed by morphometric assessment of alveolar emphysema (Figs. 11B and 12). 3R4F CS exposure resulted in increase of destructive index (DI) (Fig. 11B) and mean chord length (Fig. 12A) and led to a decrease in number density of alveoli in parenchyma and alveolar surface density in the lungs of CS-exposed mice relative to Sham-exposed mice (Fig. 12 B, C). For CHTP 1.2 and THS 2.2, these emphysema-related parameters did not differ from the Sham. Cessation and switching halted the continued increase in mean chord length, as well as the decreases in the number density of alveoli and the alveolar surface density observed in the continuous 3R4F-exposed group, approaching but not always reaching the levels of the Sham group by month 6 (Fig. 12).

3.6.6. Potential MRTPs aerosol exposure results in reduced effects in the upper respiratory tract

3R4F CS exposure induced reserve cell hyperplasia of the respiratory nasal epithelium (RNE) at nose level 1 and 2, squamous metaplasia of the RNE at nose level 1 (Fig. 13), and atrophy of the olfactory epithelium at nose level 2 at the Month 3 and Month 6 time points (no time-dependent increase) (Supplementary Figure 5). Representative images of squamous metaplasia and hyperplasia of the RNE at nose level 1 at 6 months are shown in Fig. 13C. At nose level 4, a numerical difference in the fat deposits/cholesterol clefts at the lamina propria score reached statistical significance, but the score was still in the normal range, so the effect was considered to have no biological relevance. The severity of these findings of CHTP 1.2 and THS 2.2 was strongly reduced in comparison with 3R4F CS exposure, and a minimal but statistically significant impact on reserve cell hyperplasia and/or squamous metaplasia of the RNE at nose level 1 sections was observed in response to CHTP 1.2 or THS 2.2 aerosol exposure at Month 3 of exposure (Fig. 13). However, there was no statistical significance for changes from Sham in CHTP 1.2 or THS 2.2 groups at the Month 6 time-point. Both cessation and switching resulted in a rapid recovery of squamous metaplasia toward Sham-exposed group levels within one to three months post CS-exposure (Fig. 13B). With regard to reserve cell hyperplasia, we observed an incomplete recovery within three months post CS-exposure (Fig. 13A). Overall, this histopathology evaluation of the nose revealed typical CS-related adaptive effects of the RNE in 3R4F CS-exposed mice, with much lower effects upon THS 2.2 and CHTP 1.2 aerosol exposure (Supplementary Table 6) shows results from all respiratory tract sites).

3.7. 3R4F CS exposure alters the transcriptome, proteome, miRNAome in the respiratory and cardiovascular systems of ApoE$^{-/-}$ mice

Exposure to 3R4F CS caused transcriptome alteration in respiratory and cardiovascular tissue. 3R4F CS exposure altered expression of 1,658 genes in the RNE, 4,324 genes in the lung, 578 genes in the heart ventricle, and 217 genes in the thoracic aorta after six months of exposure relative to Sham (Fig. 14A, Supplementary Figures 7-8). In contrast, neither exposure to THS 2.2 aerosol nor to CHTP 1.2 aerosol caused any significant gene expression changes relative to Sham at any time point (Fig. 14A). Smoking cessation following three months of 3R4F exposure decreased the number of differentially expressed genes (DEG) to Sham levels in all four tissues after three months of cessation (Fig. 14AB, Supplementary Figures 7-8). Switching to CHTP 1.2 also decreased the number of DEGs significantly compared with 3R4F CS exposure, but did not completely achieve the level of Cess or Sham groups. Of note, these general response patterns were also well reflected by visualizations of the global fold-change responses (Fig. 14B, Supplementary Figures 7-8).

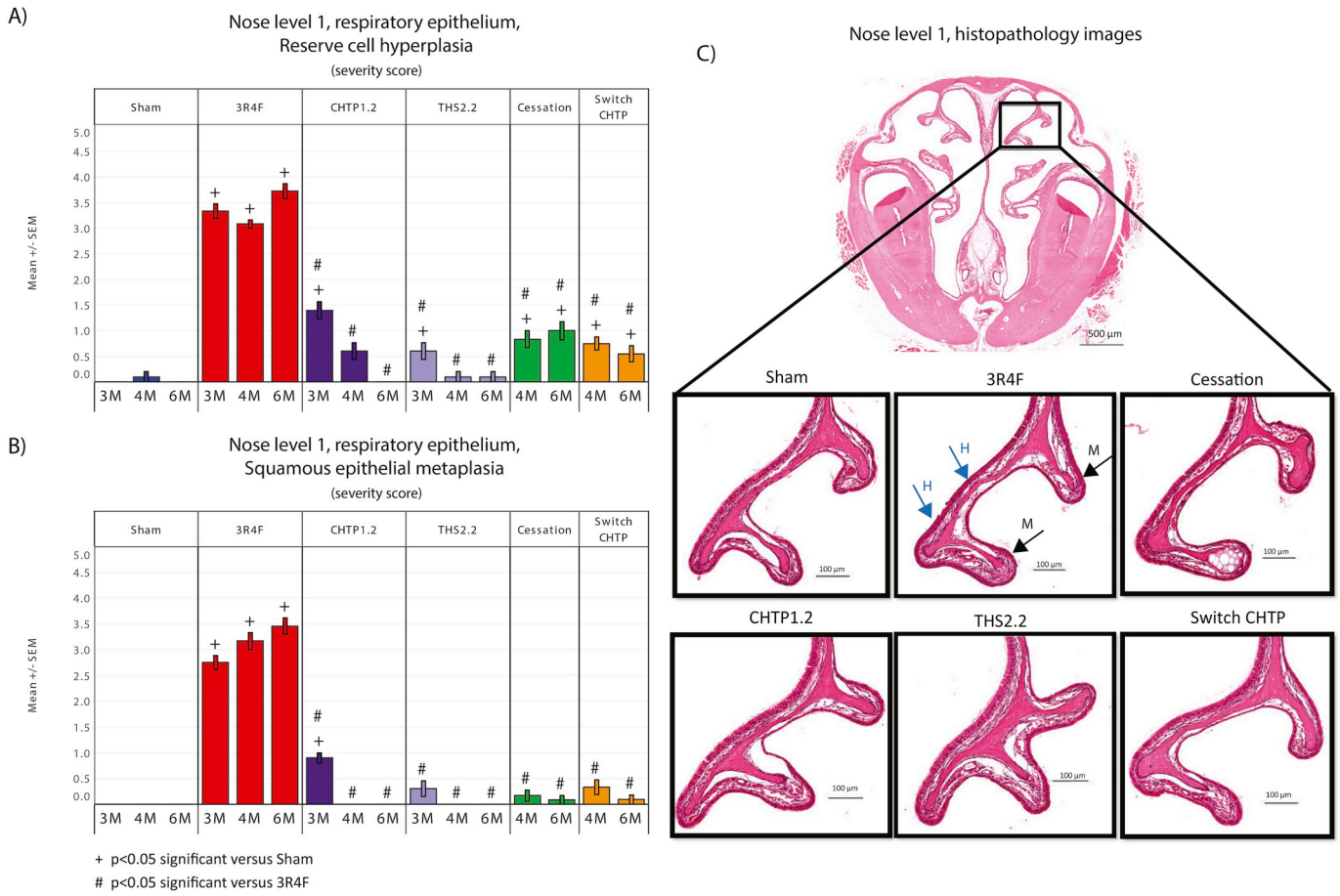

Fig. 13. Histopathological evaluation of adaptive changes of the RNE in response to 3R4F CS or MRTP aerosol exposure at Months 3, 4, and 6. Nose tissue was sectioned and stained with H&E. The impact of treatment on reserve cell hyperplasia as well as squamous epithelial metaplasia was evaluated with the scoring method at level 1–2. Histograms represent the mean score at nose level 1 for (A) Reserve cell hyperplasia and (B) Squamous epithelial metaplasia. Data are means ± SEM, n = 9–12. (C) Histologic images of nose level 1 at Month 6, 3x lens magnification, error bar equals 500 µm, black square indicates area of evaluation and magnification (naso-turbinates). (D) 20x lens magnification images representing naso-turbinates at nose level 1 in 3R4F CS- and MRTP aerosol-exposed mice, error bar equals 100 µm. Blue arrow symbols indicate hyperplasia (H). Black arrow symbols indicate squamous epithelial metaplasia (M).

Furthermore, in the lung, we observed similar systems response profiles of proteins and miRNA (Fig. 14C). Exposure to 3R4F CS resulted in a clear time-dependent effect on the lung proteome and miRNAome, with the expression of more than 400 proteins and 40 miRNA altered after six months of 3R4F CS exposure (Fig. 14C).

3.8. 3R4F CS exposure alters DNA methylation in candidate lung enhancers

We investigated DNA methylation changes at cis-regulatory elements that are promoters and candidate enhancers identified as LMRs (Supplementary Figure 1). We found that very few promoters (165 out of 23,783: 0.7%) show significant change in DNA methylation in at least one contrast (Fig. 15A, Supplementary Figure 9).

Regarding candidate enhancers (LMRs), 2,408 elements out of 121,260 (2%) showed significant change in DNA methylation in at least one contrast (Fig. 15B, Supplementary Figure 10). The vast majority of these loci were hypermethylated when compared with control samples. The 3R4F group showed the highest number of differentially methylated candidate enhancers (807: 686 hypermethylated and 121 hypomethylated) at Month 6. Samples with continuous exposure to aerosols from THS 2.2 and CHTP 1.2 at all exposure times showed a much lower number of affected loci (maximum 100 loci), similar to cessation at Months 4 and 6 and switching at Month 4. The switching group showed a high number of differentially methylated LMRs (697: 602 hypermethylated and 95 hypomethylated) at Month 6, comparable with the 3R4F profile at the same time point. 122 LMRs are commonly altered in the two groups.

3.9. Potential MRTPs aerosol exposure results in reduced inflammatory response and cell stress in the respiratory system of ApoE$^{-/-}$ mice

The causal biological network enrichment based on transcriptomics data showed aggregated perturbation of the context-relevant causal network models measured by the relative BIF (RBIF) for all exposed groups at Months 3, 4, and 6 for lung (Fig. 17A) and RNE (Fig. 18A). In lung tissue, the RBIF for 3R4F CS exposure showed a sustained trend in response to 3R4F exposure (from 100% at Month 3 to approximately 75% at Month 6), while in RNE tissue, we observed a slight impact at Months 3 and 4 of exposure and a huge effect at Month 6 of exposure (from 20% at Month 3 to approximately 100% at Month 6) (Figs. 16A–17A).

The RBIFs for the CHTP 1.2 and THS 2.2 groups remained close to 0% for the lung. The RBIF also tended to decrease upon cessation and switching; while the decrease of RBIF was complete for cessation, the switching process maintained the RBIF between 10% and 25%. For the RNE, the RBIFs do not exceed 10% for CHTP 1.2 and 20% for THS 2.2 (Fig. 17A). The RBIF tended also to decrease upon cessation and switching; while the decrease of RBIF was complete for cessation in the lung as well as in the RNE, the switching process maintained the RBIF between 10% in RNE and 25% in lung.

The network model heatmap represents the decomposition of the calculated BIF from the transcriptomics data into its mechanistic

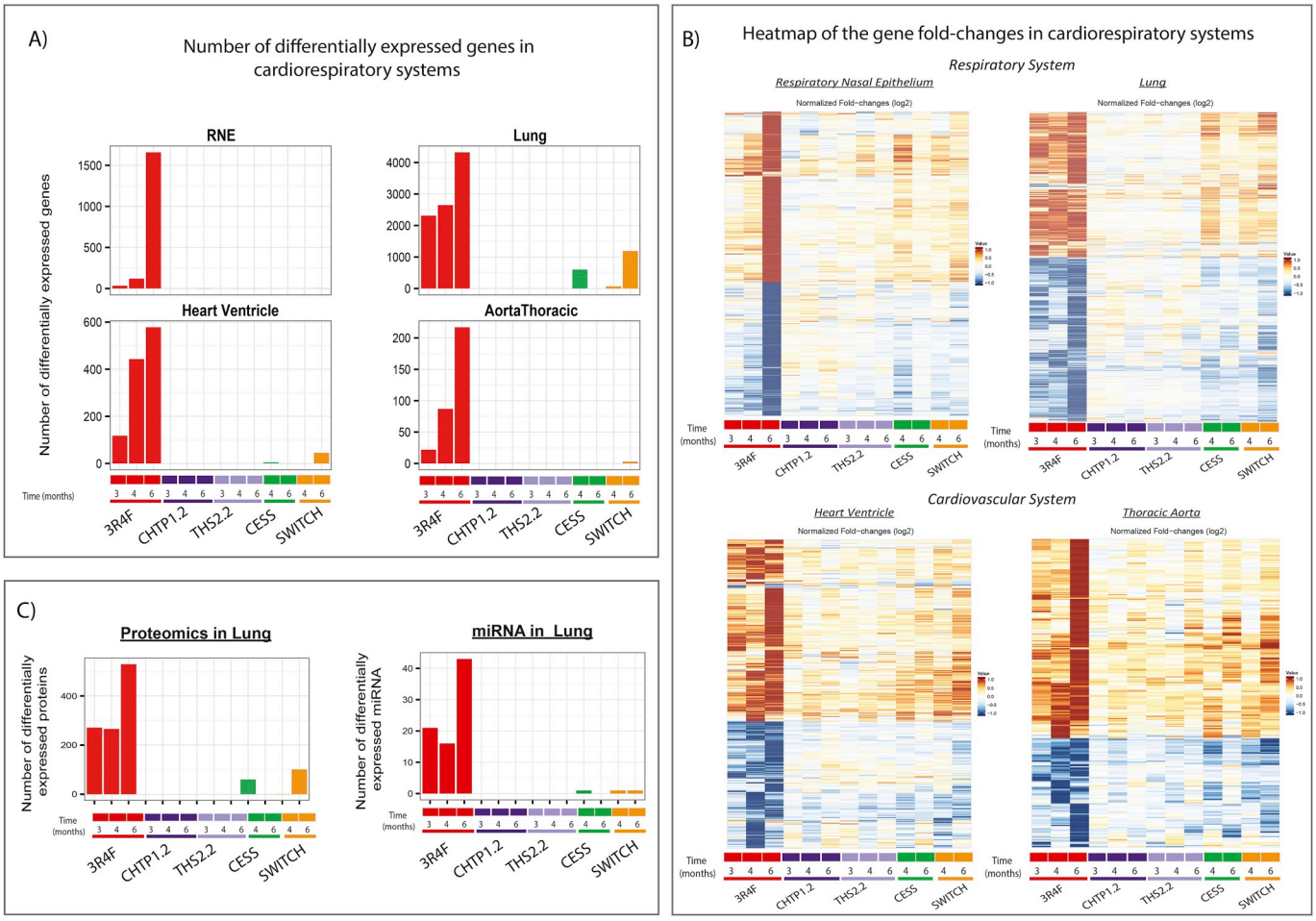

Fig. 14. Systems Toxicology – significantly regulated genes. (A) Number of DEGs for respiratory system (RNE and Lung) as well as cardiovascular system (Heart Ventricle and Aorta) analyzed tissue and exposure group, compared with the respective Sham group of the same exposure month (FDR-adjusted p-value < 0.05). (B) Heatmap of the gene fold-changes ($\log_2$, normalized to the maximum observed absolute value) that are significant in at least one comparison in respiratory (RNE-Lung) and cardiovascular (Heart Ventricle-Thoracic Aorta) tissues. Red color indicates genes that are upregulated, and blue color highlights genes that are significantly downregulated compared with the Sham group at each respective time point. (C) Changes in the lung proteome and miRNAome. Number of differentially expressed proteins and miRNA for each exposure group, compared with the respective Sham group of the same exposure month (FDR-adjusted p-value < 0.05).

components (Fig. 16B). In this heatmap, the network perturbation amplitude (NPA) scores are shown relative to the maximum value obtained in each category, thereby making also weak perturbations visible. The aggregation of separate networks under RBIF per network category demonstrate that “Cell fate and Apoptosis”, “Cell proliferation”, “Cell stress”, “Inflammatory response”, and “Tissue repair and angiogenesis” were strongly perturbed in the 3R4F group — mostly at Month 3 in the lung — and were either absent or only very weakly perturbed in the CHTP 1.2 and THS 2.2 groups over the six-month period (Fig. 16C). Similarly in the RNE, the strongest response was observed in 3R4F exposure at Month 6 (Fig. 17C). In the cessation and switching groups, the heatmap intensity coloring for each network is strongly reduced in the lung as well as in the RNE, reconfirming that cessation and switching cause less perturbation than 3R4F CS exposure (Figs. 16B–17B). The NPA score per network demonstrate that cessation and switching decrease the impact on the lung; however three months of switching to CHTP 1.2 slightly increases the cell proliferation, inflammatory process, and tissue repair and angiogenesis mechanisms (Fig. 16B).

4. Discussion

The objective of this study was to assess the impact of potential MRTPs on cardiorespiratory risk factors, such as atherosclerosis progression, lung inflammation, and respiratory system injury, in ApoE$^{-/-}$ mice following chronic exposure to 3R4F CS or potential MRTPs aerosol. The impact of cessation or switching to CHTP 1.2 aerosol was also evaluated.

Test atmosphere characterization through chemical composition analysis per chamber confirms a comparable delivery of nicotine from CHTP 1.2 and THS 2.2 aerosol as well as 3R4F CS. Surprisingly, measured levels of nicotine and cotinine in plasma were significantly higher in 3R4F CS groups than in CHTP 1.2 or THS 2.2 groups, whereas the level of total nicotine metabolites was similar between groups in urine. In previous studies of potential MRTPs, equal or even trending to higher uptake of nicotine in the potential MRTP groups had been observed, consistent with a higher respiratory minute volume due to lower irritancy of the aerosol and usually higher body weights in the MRTP groups (Coggins et al., 1989; Kogel et al., 2014; Phillips et al., 2016). In our study, the analysis of the particle size and mass in 3R4F CS and potential MRTP aerosols did not show any significant differences between MRTP aerosol and 3R4F CS, suggesting that the difference in plasma levels is not due to divergent inhalation conditions and particle properties. As the total amount of urinary metabolites accumulated within 24 h did not differ between the 3R4F CS and MRTP aerosol groups, differences in total nicotine uptake are unlikely. We speculate that the differences in blood levels seen at a single time point likely reflect contributions of dermal nicotine uptake and oral uptake by

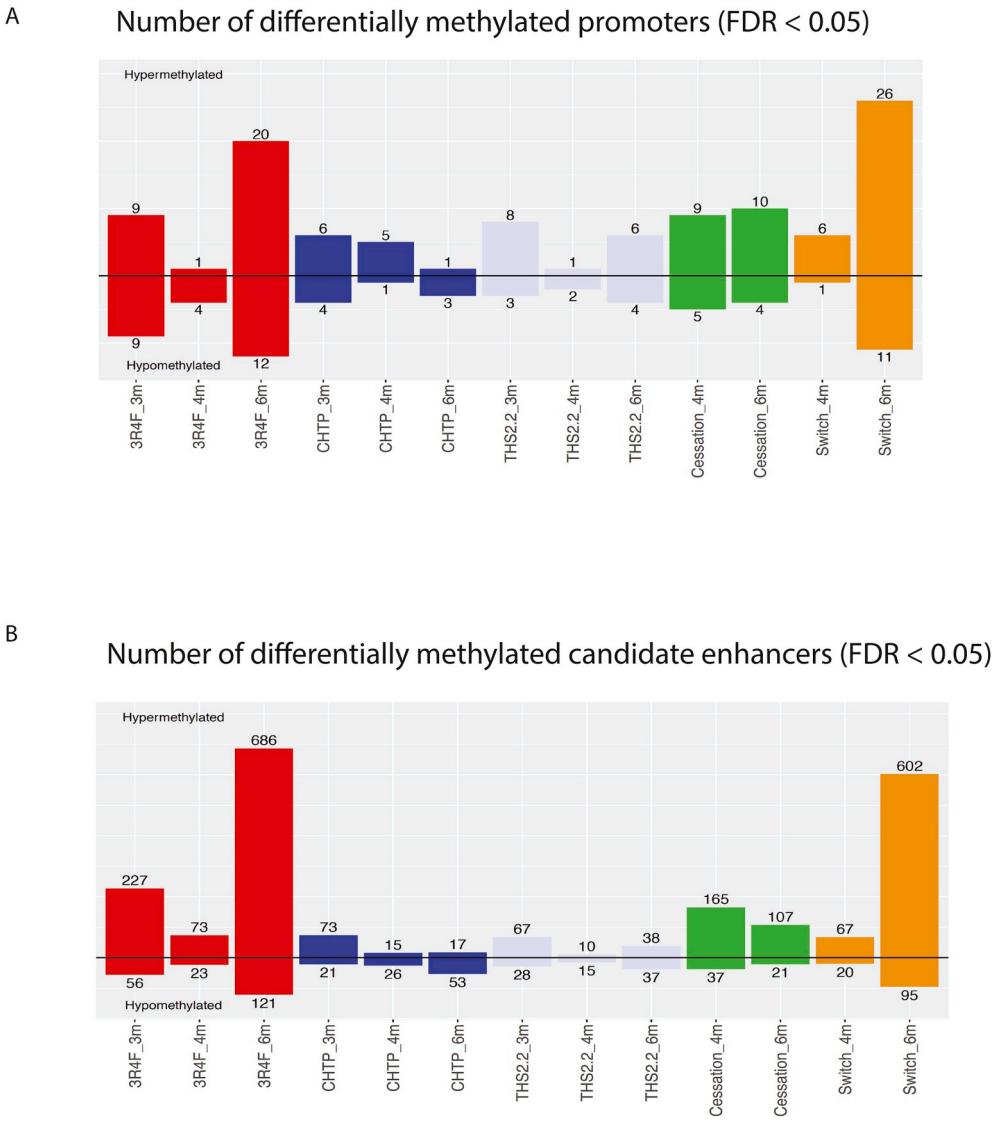

Fig. 15. Differentially methylated promoters and candidate enhancers (LMRs). (A) Barplot representing the number of differentially methylated promoters (transcription start site ± 500 bp) based on the FDR cutoff (0.05). (B) Barplot representing the number of differentially methylated candidate enhancers identified as LMRs based on the FDR cutoff (0.05). Sham samples were used as controls.

grooming (factors that cannot be excluded in whole-body inhalation studies), as well as variations in the metabolic conversion of nicotine that might depend on other physiological factors (nutrition, stress).

Our analysis demonstrated a reduced impact of the MRTPs aerosols on cardiovascular endpoints in comparison with 3R4F CS, while we observed a consistent acceleration of atherosclerotic progression in 3R4F CS-exposed mice. The plaque size observed in the aortic arch was steadily higher in 3R4F CS-exposed animals than in air-exposed animals. CHTP 1.2 and THS 2.2 aerosol-exposed mice presented reduced atherosclerotic lesion sizes compared with 3R4F CS-exposed mice. These results are in agreement with historical data showing atherosclerotic plaque enlargement following CS exposure and a reduced plaque size in response to cessation or MRTP exposure (Lietz et al., 2013; Phillips et al., 2016). In this study, the atherosclerotic plaque size was measured with two independent methods (in two separate cohorts of mice): planimetry and CT scans. Both independent methods demonstrated a significant impact of 3R4F CS on atherosclerosis progression and a reduced impact of potential MRTPs. This double analysis confirmed our previous results (Phillips et al., 2016) and allowed us to highlight that exposure to aerosols from potential MRTPs slows down the progression of atherosclerosis in ApoE$^{-/-}$ mice in a six-month exposure period in comparison with CS. While some studies demonstrated a pro-atherogenic effect of nicotine (Kilaru et al., 2001; Santanam et al., 2012), mechanistic investigations conducted in mice highlight that nicotine may promote atherosclerosis only when combined with high-fat diet supplementation (Wang et al., 2017; Wu et al., 2018).

Dyslipidemia has been shown to be one of the most potent risk factors responsible for cardiovascular events (Grundy et al., 2004; Yusuf et al., 2004). Dyslipidemia is characterized by elevated plasma cholesterol, especially total cholesterol, LDL cholesterol, and VLDL cholesterol levels. In our study, the 3R4F CS-exposed mice exhibited marked increases in serum levels of total cholesterol and VLDL cholesterol at Months 2, 3, and 4 of exposure; both are important cardiovascular risk factors (Carmena et al., 2004). The increase of lipids in blood could be due to an increase in lipolysis in response to 3R4F CS (Hofstetter et al., 1986). It has been shown that cigarette smoking increases free fatty acid (FFA) and circulating FFA concentrations. In humans, cigarette smoking augmented delivery of FFA to the liver, amplified hepatic reesterification of FFA, and boosted VLDL secretion (Hellerstein et al., 1994). In ApoE$^{-/-}$ mice, dyslipidemia is even aggravated by the impairment of VLDL re-uptake in the liver (Lo Sasso

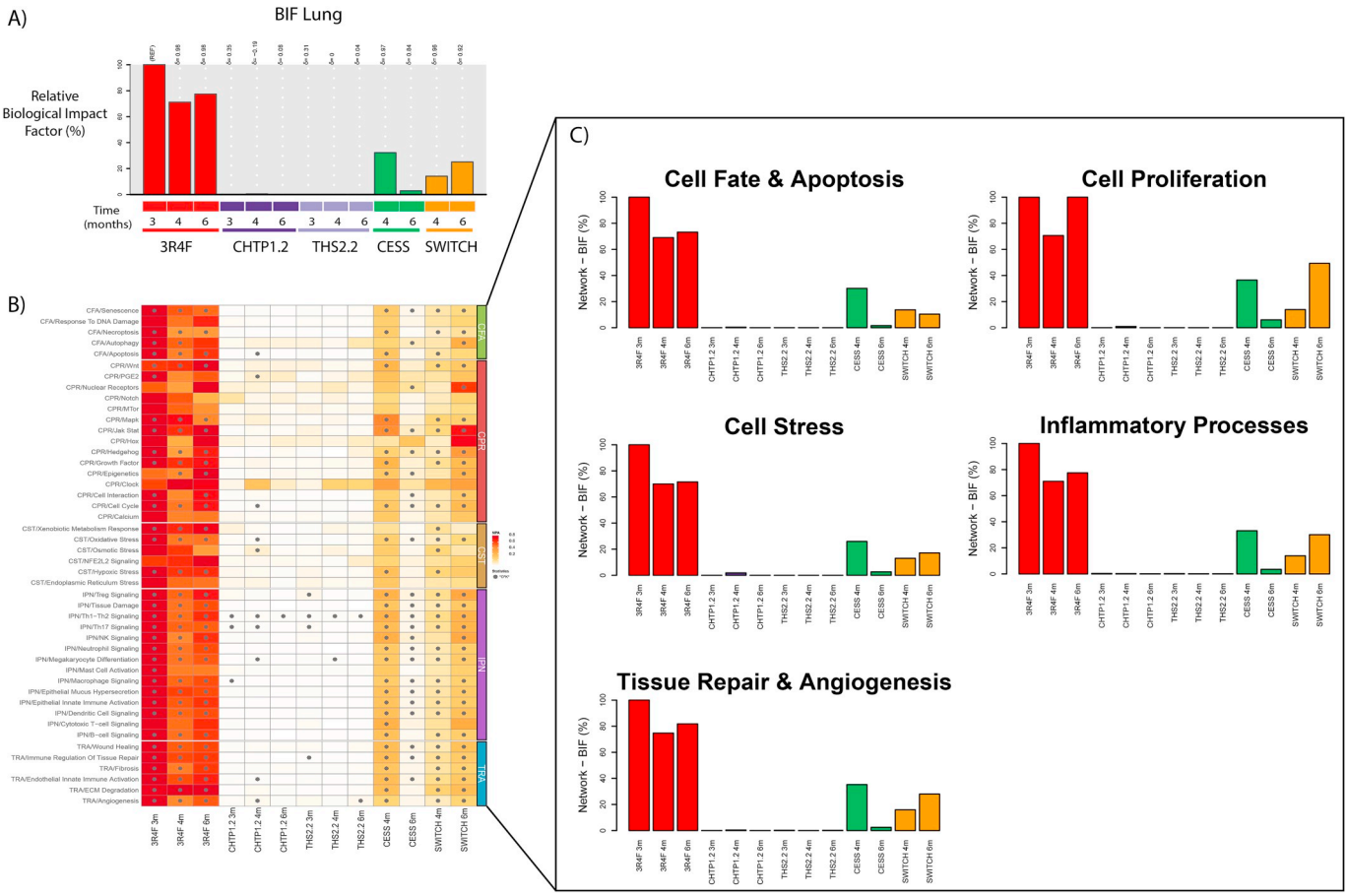

Fig. 16. Network-based BIF and NPA analysis from the lung. (A) RBIF for treatment versus Sham. The percentages show the RBIF, which is derived from the cumulated network perturbations caused by the treatment relative to the reference, defined as the treatment comparison showing the highest perturbation (i.e., at the Month 6 time point). (B) Heatmap of NPA scores summarizing subnetwork NPAs relative to the maximum NPA in each subnetwork. Stars indicate significant perturbations: a network is considered as perturbed if, in addition to the significance of the NPA score with respect to the experimental variation, the two companion statistics (O and K) derived to inform on the specificity of the NPA score with respect to the biology described in the network, are significant. *O and K statistic *p*-values below 0.05 and significant with respect to the experimental variation. (C) Network-BIF demonstrates the level of the perturbation in response to 3R4F CS and heat-not-burn products in lung tissue.

et al., 2016). Despite the different mechanisms involved in dyslipidemia of mice and humans, our results are aligned with reports in the literature, demonstrating an impact of CS exposure on cholesterol in lipoprotein particles such as VLDL and LDL (Gastaldelli et al., 2010; Rao Ch and Subash, 2013). Contrary to 3R4F CS, MRTP aerosol exposure did not affect LDL or VLDL cholesterol levels over six months of exposure. Smoking cessation as well as THS 2.2 exposure increased HDL cholesterol. The increase of HDL is in agreement with previous clinical studies, which showed that smoking cessation improved the plasma HDL profile (Gepner et al., 2011). Lipoproteins play a fundamental role in atherosclerosis, and their interaction with the arterial wall appears to initiate the cascade of events that leads to atherosclerosis (Ference et al., 2017). In our study, we observed the alteration of lipid profiles and an increase in atherosclerosis progression in 3R4F CS-exposed animals, suggesting that the increase in lipid levels could contribute to atherosclerosis progression. An impact of 3R4F CS exposure on the cardiovascular system was also supported by the transcriptomics analyses of thoracic aorta and heart left ventricle, which demonstrated a strong differential expression response that intensified at Month 6 of exposure. In contrast, exposure to aerosols from both MRTPs resulted in an attenuated atherosclerotic progression, associated with much more limited effects on the transcriptomes of these cardiovascular tissues. Together, these data demonstrated a substantial impact of 3R4F CS on the cardiovascular system of ApoE$^{-/-}$ mice, which is much lower for THS 2.2 and CHTP 1.2.

Histopathological changes caused by CS smoke in the respiratory tract of rodents have been studied in depth (Hamm et al., 2007; Kogel et al., 2014; Stinn et al., 2010; Terpstra et al., 2003; Werley et al., 2008). Hamm et al. and others demonstrated that exposure to CS is associated with hyperplasia, metaplasia, and inflammation of the RNE (Hamm et al., 2007; Kogel et al., 2014; Stinn et al., 2010; Terpstra et al., 2003; Werley et al., 2008). In our study, we observed moderate to marked reserve cell hyperplasia and squamous metaplasia of the RNE at nose level 1, minimal but statistically significant hyperplasia at nose level 2, and mild atrophy of the olfactory epithelium at nose level 2 in response to 3R4F CS exposure. This response was consistent with the typical CS exposure-related adaptive effects of the rodent RNE described previously (Kogel et al., 2014; Stinn et al., 2010; Terpstra et al., 2003; Werley et al., 2008). Also, as observed previously, these adaptive changes were entirely resolved for squamous metaplasia or strongly diminished for hyperplasia parameter upon 3R4F CS cessation. The THS 2.2 aerosol did not elicit changes except from mild reserve cell hyperplasia at nose level 1 (the most sensitive site), seen initially (Month 3), that was subsequently resolved at Months 4 and 6, consistent with an adaptation to low-grade irritation. A similar response pattern was observed for CHTP 1.2 aerosol exposure, with a transient weak effect on both endpoints at Month 3 that disappeared at the follow-up time points. The effects from switching from 3R4F CS to CHTP 1.2 aerosol were similar to those from switching from 3R4F CS to fresh air (cessation) or to Sham exposure (for metaplasia). While the RNE tissue

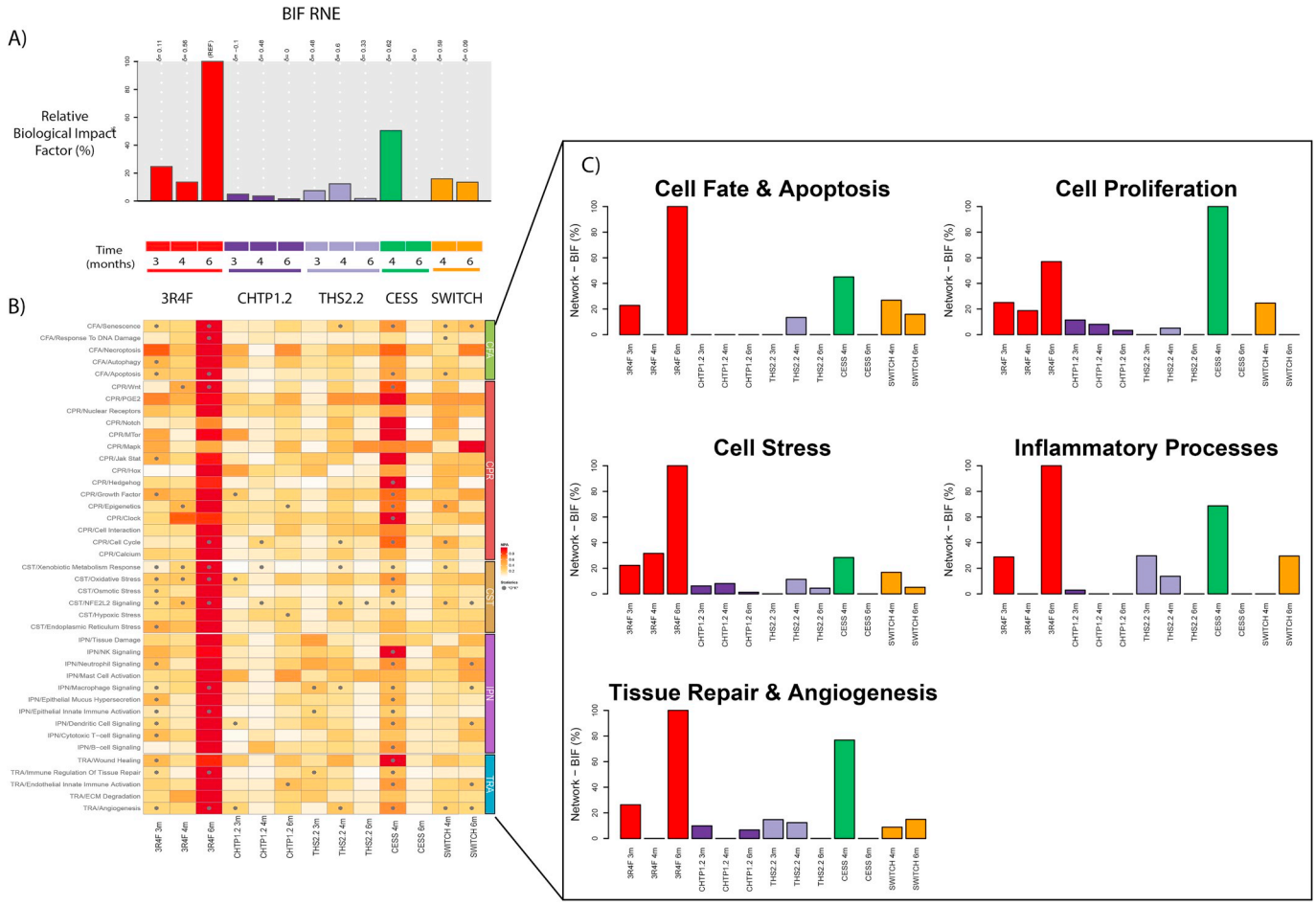

Fig. 17. Network-based BIF and NPA analysis from the RNE. (A) RBIF for treatment versus Sham. The percentages show the RBIF, which is derived from the cumulated network perturbations caused by the treatment relative to the reference, defined as the treatment comparison showing the highest perturbation (i.e., at the Month 6 time point). (B) Heatmap of NPA scores summarizing subnetwork NPAs relative to the maximum NPA in each subnetwork. Stars indicate significant perturbations: a network is considered as perturbed if, in addition to the significance of the NPA score with respect to the experimental variation, the two companion statistics (O and K) derived to inform on the specificity of the NPA score with respect to the biology described in the network, are significant. (C) Network-BIF demonstrates the level of the perturbation in response to 3R4F CS and heat-not-burn products in RNE tissue.

showed only adaptive changes in response to 3R4F CS that were partially reversible (cessation group), the effect of THS 2.2 and CHTP 1.2 aerosol was marginal, and switching to CHTP 1.2 after three months led to similar recovery as switching to fresh air.

In response to 3R4F CS exposure but not to MRTP aerosol exposure, more sustained inflammatory changes were observed and supported by multiple parameters determined in the lung. The recruitment of inflammatory cells, in particular macrophages and neutrophils, was accompanied by an increase of inflammatory cytokines and chemokines in BALF. Together, these data indicate that exposure to 3R4F CS, in contrast to CHTP 1.2 or THS 2.2 aerosols, leads to pronounced lung inflammation, which could trigger ECM destruction and development of emphysema (Foronjy et al., 2008). Scientific literature demonstrates that chronic inflammation is essential for the development of emphysema. Accumulation and activation of immune cells, such as neutrophils and macrophages, contribute to lung injury and serve as a self-perpetuating stimulus for further immune activation (Sharafkhaneh et al., 2008; Tuder et al., 2003). The mobilization of inflammatory cells to the lung leads to the release of potentially destructive mediators, including tissue proteases and cytokines, which contribute directly to tissue remodeling and destruction (Saetta et al., 2001). MRTP aerosol exposure was associated with considerably lower inflammatory cell infiltration and activation and thus may reduce risk of developing emphysema, as supported by the lower emphysematous changes in these groups.

Progressive lung injury observed through emphysematous changes in 3R4F CS-exposed mice was indicated by various endpoints, such as lung volume and lung function, as well as histopathology and morphometry analysis. 3R4F CS-exposed mice showed significantly increased lung inflammation. Moreover, we could observe a decrease in the number of alveoli and alveolar surface density and an increase in DI and mean chord length, which are featured characteristics of lung emphysematous changes (Sharafkhaneh et al., 2008; Tuder et al., 2003). Lung inflammation and alveolar damage were attenuated significantly (compared with continued 3R4F CS exposure) after smoking cessation or switching to CHTP 1.2, which supported halting the progression of initial emphysematous changes after stopping 3R4F CS exposure. Lung function, as assessed through PVs-P loops, demonstrated significant increases in shift as well as in lung volume under static pressure in response to 3R4F CS exposure. In contrast, no such effect occurred following CHTP 1.2 or THS 2.2 aerosol exposure, and switching to CHTP 1.2 aerosol had the same effect as switching to fresh air on the partial recovery from inflammation or on halting the progression of emphysematous changes. Taken together, potential MRTP aerosol exposure, in contrast to 3R4F CS, was associated with no significant effects on inflammatory cell infiltration and activation, inflammatory mediator secretion, and emphysematous changes in lung tissue.

The measured apical endpoints (e.g., histopathology, BALF cytokines, aortic plaque size) are well aligned with results from molecular

A)

	Current study	Phillips et al. 2016
Test system	Female Apoe-/- mice	Female Apoe-/- mice
Total duration (dissection time points) [months]	6 (2,3,4,6)	8 (1,2,3,6,8)
Exposure schedule	3 h per day, 5 days per week	3 h per day, 5 days per week
Exposure groups	Sham	Sham
	3R4F (28 μg nicotine /L)	3R4F (29.9 μg nicotine /L)
	CHTP1.2 (28 μg nicotine /L)	THS2.2 (29.9 μg nicotine /L)
	THS2.2 (28 μg nicotine /L)	Cessation (after 2mo 3R4F)
	Cessation (after 3mo 3R4F)	Switch to THS2.2 (after 2mo 3R4F)
	Switch to CHTP1.2 (after 3mo 3R4F)	

B)

C)

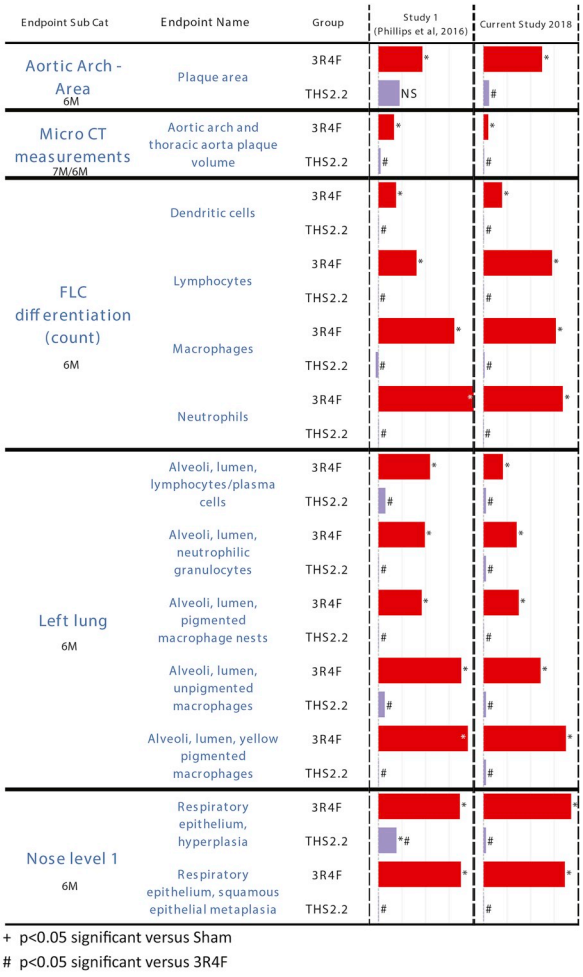

Fig. 18. Comparison of current and previous ApoE$^{-/-}$ assessment studies. (A) Comparison of the study design between the current and previous ApoE$^{-/-}$ studies (Phillips et al., 2015, 2016). (B) Biomarkers of CS exposure quantification in current and previous ApoE$^{-/-}$ studies at Months 5 and 6 of exposure. Relative values to the Sham group are presented (i.e., mean value of exposure group minus mean value of Sham group). (C) Comparison of the impact of 3R4F CS and THS 2.2 exposure on disease endpoints, such as atherosclerotic plaque progression, inflammatory cell infiltration in the lung, nose hyperplasia, and metaplasia, between current and previous ApoE$^{-/-}$ studies at Months 6 and 7 of exposure. Relative values to the Sham group are presented. + $p < 0.05$ significant versus Sham group; #, $p < 0.05$ significant versus 3R4F group.

analysis. Transcriptomic and proteomics analysis confirmed the strong impact of 3R4F exposure on the respiratory and cardiovascular system and, in addition to the inflammatory response, revealed induction of an oxidative stress response and apoptosis in lung tissue upon 3R4F CS exposure, whereas potential MRTP aerosols elicited much lower effects. Molecular focusing on the lung tissue demonstrates that cell stress networks as well as key genes and proteins involved in the oxidative response were dysregulated in response to 3R4F CS. Oxidative stress caused by CS inhalation plays a significant role in generating emphysema (Rangasamy et al., 2004, 2009). A major consequence of oxidative stress is activation of the transcription factor nuclear factor-κB, which activates proinflammatory cytokine transcription (Rahman and Kilty, 2006; Seagrave et al., 2004; Sharafkhaneh et al., 2008; Yang et al., 2006). Our results are well aligned with scientific literature, which demonstrated an impact of CS on lung inflammation and stress response (Braber et al., 2010; Bracke et al., 2006; Thatcher et al., 2005). Moreover, our results are comparable with previously observed changes in response to 3R4F CS exposure in ApoE$^{-/-}$ and C57BL/6 mice (Boue et al., 2013; Phillips et al., 2015). Smoking cessation or switching decrease pulmonary inflammation as well as cell stress by suppressing inflammatory cell infiltration and inflammatory mediator secretion. In general, these results were fully supported by the numbers of neutrophils, macrophages, and lymphocytes observed in the histological sections of the lung as well as the molecular analysis provided by transcriptomics, proteomics, and miRNA analysis. There was an unexpectedly high level of response in several molecular endpoints generated from the six-month switching/omics cohort of mice when compared with the initial decrease at the Month 4 time point (i.e., one month after switching), which was particularly evident for DNA methylation profiles (number of differentially methylated candidate enhancers in the lung) as well as for transcriptomics (number and fold-changes of DEGs in lung and heart ventricle) and proteomics (number and fold-changes of DEGs in lung tissue). Given the absence of such a biphasic response at the Month 4 and Month 6 time points for the apical endpoints in the switching groups that were assessed in a different cohort of mice, we believe that technical reasons rather than biological effects may underlie the enhanced response profiles.

The impact of THS 2.2 aerosol on cardiovascular and respiratory systems, compared with that of 3R4F CS, was also evaluated in our previous ApoE$^{-/-}$ mice study (Phillips et al., 2015). The overall study design and exposure conditions were comparable, with slight differences in the switching time point, exposure time point, and products compared. In our previous study, the exposure duration was set to eight months, whereas in the current study, the last time point corresponds to six months of exposure. The switching was also postponed for one month (switching set at three months of exposure in this study instead

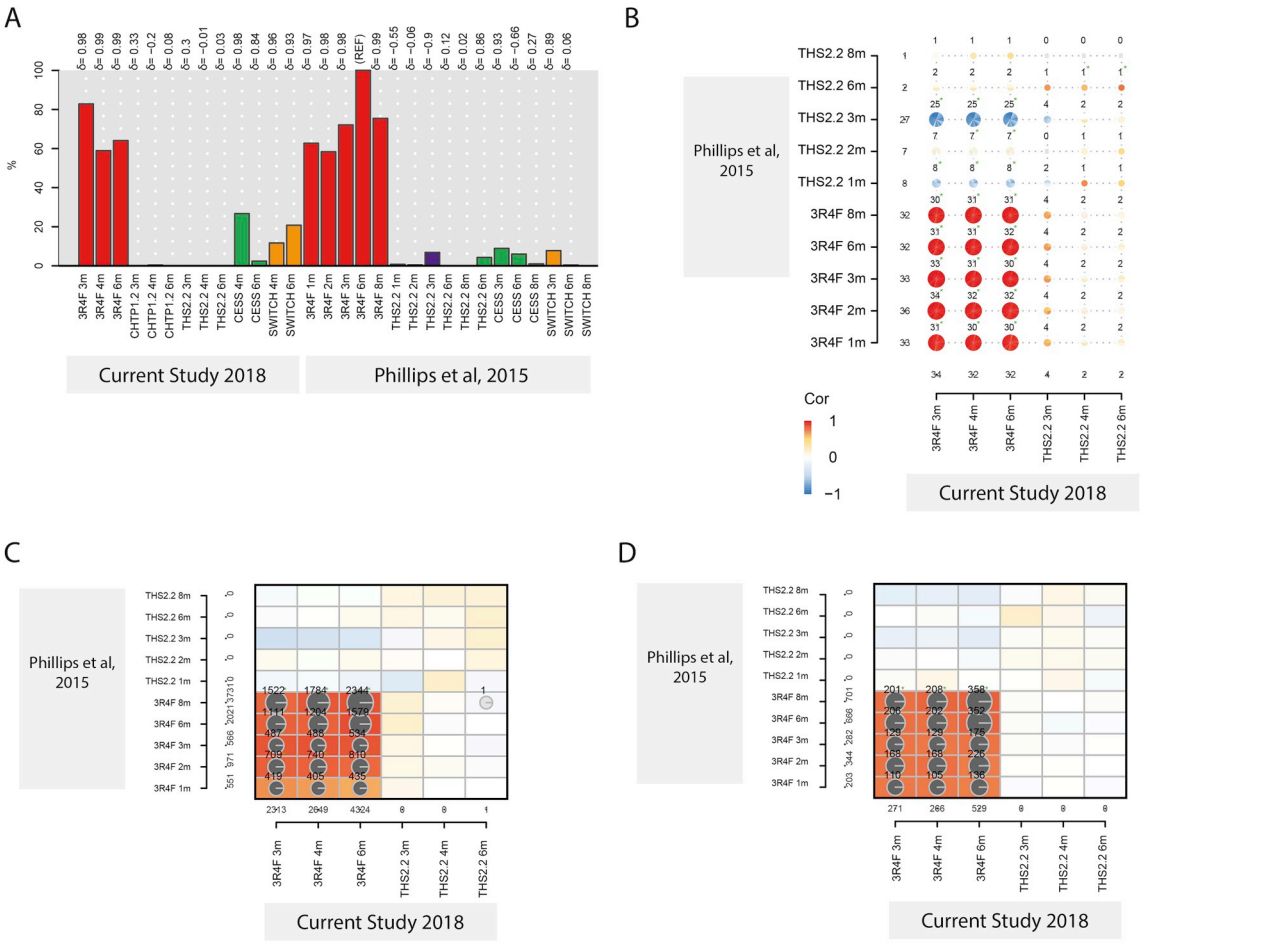

(caption on next page)

Fig. 19. Comparison of molecular exposure effects on the lung in current and previous ApoE$^{-/-}$ assessment studies. Molecular responses are compared between the current study and the previous ApoE$^{-/-}$ study (Phillips et al., 2015, 2016). (A) BIF analysis. The percentages give the biological impact relative to the reference with the highest perturbation (REF). δ (from −1 to 1) indicates how similar the underlying network perturbations are with respect to the reference (i.e., REF). (B) Network-level comparison. Number of perturbed and shared perturbed networks is indicated for each comparison; the color-scale in the inner pie represents the correlation between network backbone scores. (C–D) Differential gene (C) and protein (D) expression comparisons for the 3R4F CS and THS 2.2 groups in both studies. Correlation coefficients are color coded (see key). The numbers of overlapping differentially abundant genes/proteins are indicated in each cell (with consistency of the change in direction indicated by the pie chart; see key). Green stars indicate significance of a Fisher association test ($p < 0.05$). (E–F) Comparison of the gene (E) and protein (F) $\log_2$ fold-changes for the 3R4F CS and THS 2.2 groups (versus Sham) shared between both studies. Genes/proteins with significant differential expression in either study are marked by larger dots; Pearson correlation coefficients for all (R_{all}^2) and the differentially expressed (R_{sig}^2) genes/proteins are indicated, with the linear fit for the significant genes/proteins shown by a red regression line. Note that only if 10 or more genes/proteins were significantly differentially expressed, the R_{sig}^2 was calculated, and the regression line was included.

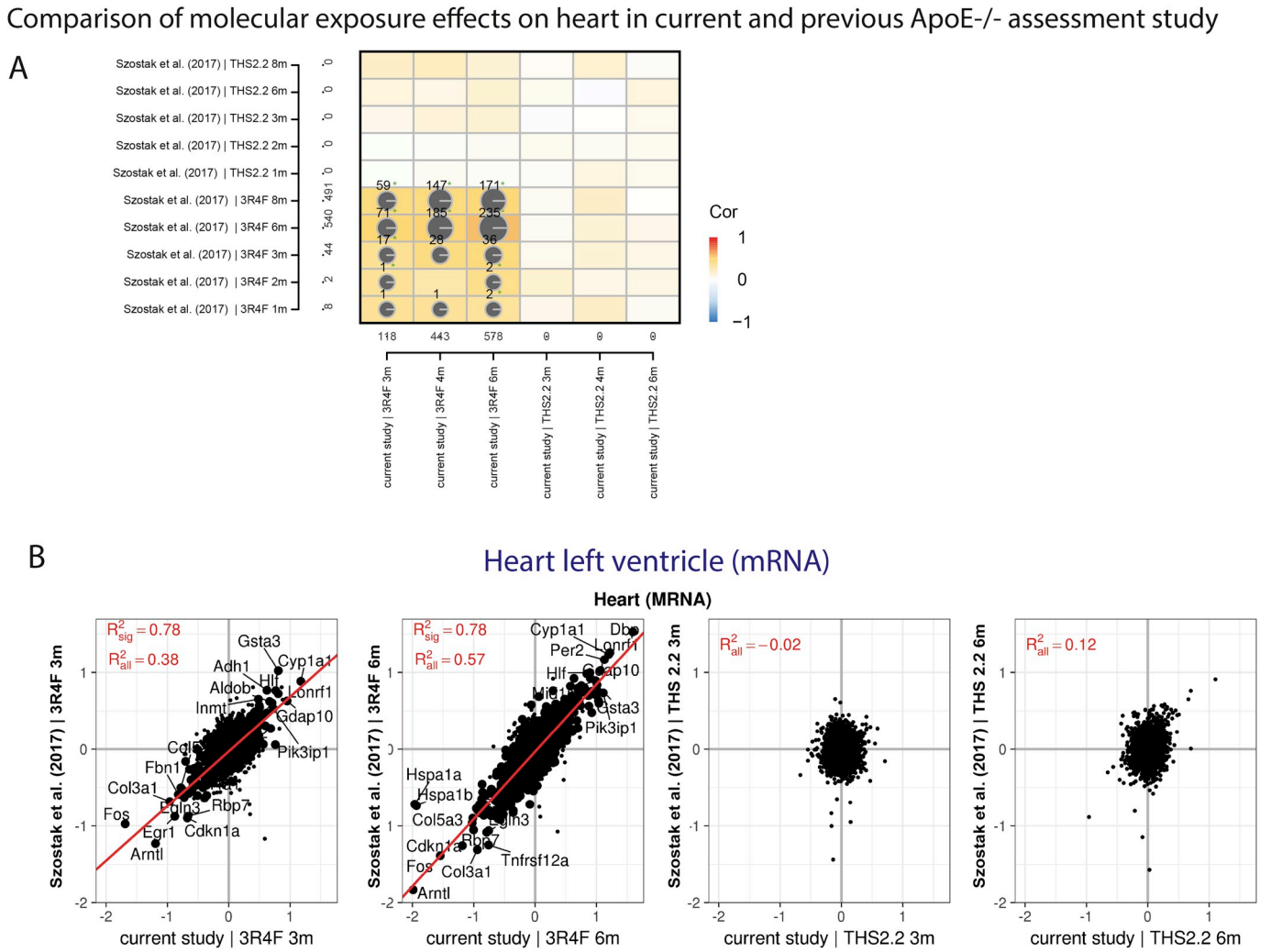

Fig. 20. Comparison of molecular exposure effects on the heart in current and previous ApoE$^{-/-}$ assessment studies. Differential gene and protein expression comparisons for the 3R4F CS and THS 2.2 groups in both studies. (A) Heart transcriptomics. (B) Correlation coefficients are color coded (see key). The numbers of overlapping differentially abundant genes/proteins are indicated in each cell (with consistency of the change in direction indicated by the pie chart; see key). Green stars indicate significance of a Fisher association test ($p < 0.05$).

of two months) (Phillips et al., 2015). In our previous study, we analyzed the impact of THS 2.2, whereas the current study evaluated the impact of two heat-not-burn tobacco products, CHTP 1.2 and THS 2.2 (Fig. 18A). Comparison between both studies (for THS 2.2 versus 3R4F CS) demonstrated a similar reduction, of the uptake of HPHCs (Fig. 18B), and of effects such as atherosclerosis progression, lung inflammation, and nose hyperplasia and metaplasia (Fig. 18C).

Molecular response profiles were also found to be similar between the "Eight month study" (Phillips et al., 2015) and the current one "Six month study". In the lung, 3R4F CS elicited a clear and consistent effect on causal biological networks across both studies (Fig. 19). The BIF showed a similar amplitude of the molecular biological responses upon 3R4F CS exposure, and the biological network responses were strongly correlated for 3R4F CS across all commonly investigated exposure time points (Fig. 19C and D). Both the lung transcriptome and the proteome response to 3R4F CS exposure demonstrated highly correlated fold-changes and shared DEGs and proteins. For example, 78% (67%) of the DEGs (proteins) were shared after six months of exposure to 3R4F CS in both studies. Moreover, significantly expressed genes (proteins) at this time point in either study demonstrated a Pearson correlation

coefficient between the $\log_2$ fold-changes of $R_{sig}^2 = 0.85$ (0.75), further corroborating the high reproducibility of these molecular exposure responses to 3R4F CS in the lung (comparing results from two studies that were conducted approximately four years apart). The transcriptome response in heart tissue was also well reproduced between the studies (Szostak et al., 2017): 44% of the DEGs for 3R4F at Month 6 were shared between both studies, with a Pearson correlation coefficient of $R_{sig}^2 = 0.78$ (Fig. 20). In contrast, reflecting the very low to absent biological responses upon THS 2.2 exposure, correlation of the THS 2.2 groups between the studies was also low to absent. More details and additional molecular analyses will be provided elsewhere.

Taken together, these results support the robustness of the conducted exposure response measurements for both the classical and the omics endpoints. Although, due to the overall low to absent THS 2.2 effects, these comparisons do not allow a direct numerical comparison between both studies, these comparisons highlight the consistent reduction of biological exposure effects for THS 2.2 compared with 3R4F in both studies, seen as absence of significant effects, while the sensitivity for the positive control, 3R4F CS, was comparable across the studies. In both studies, molecular responses to THS 2.2 and 3R4F exposure were not correlated, further supporting the consistent absence of 3R4F CS exposure-related effects upon exposure to THS 2.2 aerosol. In this context, the observed similar reductions in biological effects for THS 2.2 and CHTP 1.2 aerosols further validate the heat-not-burn principle, demonstrating that reduced HPHC levels in the aerosol – due to heating rather than burning tobacco – consistently translate into reduced biological effects caused by these HPHCs.

Moreover, the observed reduction in biological effects following exposure of mice to aerosols from THS 2.2 and CHTP 1.2 in comparison to CS at a comparable level of nicotine is consistent with the concepts of tobacco harm reduction based on “providing smokers with the nicotine to which they are addicted without the tobacco smoke that is responsible for almost all of the harm caused by smoking” (Royal College of Physicians, 2007, 2016) and the low hazard of nicotine when decoupled from combustion or other toxic modes of delivery (Niaura, 2016).

5. Conclusions

This study demonstrated a clear impact of 3R4F CS on the cardiovascular and respiratory system of $ApoE^{-/-}$ mice. CS accelerated the development of atherosclerotic plaques and caused inflammation and emphysematous changes, as demonstrated by a number of anatomical and molecular disease indicators. Conversely, chronic exposure of mice to CHTP 1.2 or THS 2.2 aerosol (with nicotine concentration matched to 3R4F CS) had minimal biological impact on disease endpoints and weak effects on molecular endpoints. Switching to CHTP 1.2 aerosol and cessation equally resulted in partial recovery to Sham-exposed levels (nasal adaptive changes, lung function, lung inflammation, atherosclerotic plaque area). Overall, this systems toxicology study investigated the impact of potential MRTPs on both respiratory and cardiovascular systems. Our apical and molecular analyses highlight a reduced impact of potential MRTPs on cardiovascular and respiratory systems compared with continuous smoking.

Funding

All authors except WKS and AB are employees of Philip Morris International. Philip Morris International is the sole source of funding and sponsor of this study.

Acknowledgments

The authors wish to acknowledge and thank the members of the bioresearch and aerosol generation teams at PMIRL-S for their technical contributions. A particular thanks to Stephanie Boue for her help.

Appendix A. Supplementary data

Supplementary data to this article can be found online at https://doi.org/10.1016/j.fct.2019.02.008.

Transparency document

Transparency document related to this article can be found online at https://doi.org/10.1016/j.fct.2019.02.008.

References

Ansari, S., Baumer, K., Boue, S., Dijon, S., Dulize, R., Ekroos, K., Elamin, A., Foong, C., Guedj, E., Hoeng, J., Ivanov, N.V., Krishnan, S., Leroy, P., Martin, F., Merg, C., Peck, M.J., Peitsch, M.C., Phillips, B., Schlage, W.K., Schneider, T., Talikka, M., Titz, B., Vanscheeuwijck, P., Veljkovic, E., Vihervaara, T., Vuillaume, G., Woon, C.Q., 2016. Comprehensive systems biology analysis of a 7-month cigarette smoke inhalation study in C57BL/6 mice. Scientific data 3, 150077.

Arunachalam, G., Sundar, I.K., Hwang, J.W., Yao, H., Rahman, I., 2010. Emphysema is associated with increased inflammation in lungs of atherosclerosis-prone mice by cigarette smoke: implications in comorbidities of COPD. J. Inflamm. 7, 34.

Attard, R., Dingli, P., Doggen, C.J.M., Cassar, K., Farrugia, R., Wettinger, S.B., 2017. The impact of passive and active smoking on inflammation, lipid profile and the risk of myocardial infarction. Open Heart 4, e000620.

Boue, S., De Leon, H., Schlage, W.K., Peck, M.J., Weiler, H., Berges, A., Vuillaume, G., Martin, F., Friedrichs, B., Lebrun, S., Meurrens, K., Schracke, N., Moehring, M., Steffen, Y., Schueller, J., Vanscheeuwijck, P., Peitsch, M.C., Hoeng, J., 2013. Cigarette smoke induces molecular responses in respiratory tissues of $ApoE^{-/-}$ mice that are progressively deactivated upon cessation. Toxicology 314, 112–124.

Boue, S., Talikka, M., Westra, J.W., Hayes, W., di Fabio, A., Park, J., Schlage, W.K., Sewer, A., Fields, B., Ansari, S., Martin, F., Veljkovic, E., Kenney, R., Peitsch, M.C., Hoeng, J., 2015. Causal biological network database: a comprehensive platform of causal biological network models focused on the pulmonary and vascular systems. Database. J. Biol. databases and curation bav030 2015.

Boue, S., Tarasov, K., Janis, M., Lebrun, S., Hurme, R., Schlage, W., Lietz, M., Vuillaume, G., Ekroos, K., Steffen, Y., Peitsch, M.C., Laaksonen, R., Hoeng, J., 2012. Modulation of atherogenic lipidome by cigarette smoke in apolipoprotein E-deficient mice. Atherosclerosis 225, 328–334.

Braber, S., Henricks, P.A., Nijkamp, F.P., Kraneveld, A.D., Folkerts, G., 2010. Inflammatory changes in the airways of mice caused by cigarette smoke exposure are only partially reversed after smoking cessation. Respir. Res. 11, 99.

Bracke, K.R., D'Hulst A, I., Maes, T., Moerloose, K.B., Demedts, I.K., Lebecque, S., Joos, G.F., Brusselle, G.G., 2006. Cigarette smoke-induced pulmonary inflammation and emphysema are attenuated in CCR6-deficient mice. J. Immunol. 177, 4350–4359.

Burger, L., Gaidatzis, D., Schubeler, D., Stadler, M.B., 2013. Identification of active regulatory regions from DNA methylation data. Nucleic Acids Res. 41, e155.

Carmena, R., Duriez, P., Fruchart, J.C., 2004. Atherogenic lipoprotein particles in atherosclerosis. Circulation 109, III2–7.

Centers for Disease, C., Prevention, 2008. Smoking-attributable mortality, years of potential life lost, and productivity losses–United States, 2000-2004. MMWR Morb. Mortal. Wkly. Rep. 57, 1226–1228.

Cho, M.H., Lee, K., Park, S.M., Chang, J., Choi, S., Kim, K., Koo, H.Y., Jun, J.H., Kim, S.M., 2018. Effects of smoking habit change on all-cause mortality and cardiovascular diseases among patients with newly diagnosed diabetes in Korea. Sci. Rep. 8, 5316.

Coggins, C.R., Ayres, P.H., Mosberg, A.T., Sagartz, J.W., Burger, G.T., Hayes, A.W., 1989. Ninety-day inhalation study in rats, comparing smoke from cigarettes that heat tobacco with those that burn tobacco. Fundam. Appl. Toxicol. 13, 460–483.

Ezzati, M., Henley, S.J., Thun, M.J., Lopez, A.D., 2005. Role of smoking in global and regional cardiovascular mortality. Circulation 112, 489–497.

FDA, 2015. Comments of the National Institute for Occupational Safety and Health to the Food and Drug Administration (FDA) in Response to Establishment of Public Docket; Electronic Cigarettes and the Public Health Workshop. Docket no FDA-2014-N-1936.

Ference, B.A., Ginsberg, H.N., Graham, I., Ray, K.K., Packard, C.J., Bruckert, E., Hegele, R.A., Krauss, R.M., Raal, F.J., Schunkert, H., Watts, G.F., Boren, J., Fazio, S., Horton, J.D., Masana, L., Nicholls, S.J., Nordestgaard, B.G., van de Sluis, B., Taskinen, M.R., Tokgozoglu, L., Landmesser, U., Laufs, U., Wiklund, O., Stock, J.K., Chapman, M.J., Catapano, A.L., 2017. Low-density lipoproteins cause atherosclerotic cardiovascular disease. 1. Evidence from genetic, epidemiologic, and clinical studies. A consensus statement from the European Atherosclerosis Society Consensus Panel. Eur. Heart J. 38, 2459–2472.

Food and Drug Administration, F., 2012a. Federal food, Drug, and cosmetic act. In: 18 FDC Act as Amended by the Family Smoking Prevention and Tobacco Control Act (Public Law 111-31). F. Food and Drug Administration, pp. 21 U.S.C 387 k.

Food and Drug Administration, F., 2012b. Modified Risk Tobacco Product Applications: Draft Guidance for Industry.

Foronjy, R., Nkyimbeng, T., Wallace, A., Thankachen, J., Okada, Y., Lemaitre, V., D'Armiento, J., 2008. Transgenic expression of matrix metalloproteinase-9 causes adult-onset emphysema in mice associated with the loss of alveolar elastin. Am. J. Physiol. Lung Cell Mol. Physiol. 294, L1149–L1157.

Gaidatzis, D., Lerch, A., Hahne, F., Stadler, M.B., 2015. QuasR: quantification and annotation of short reads in R. Bioinformatics 31, 1130–1132.

Gastaldelli, A., Folli, F., Maffei, S., 2010. Impact of tobacco smoking on lipid metabolism,

body weight and cardiometabolic risk. Curr. Pharmaceut. Des. 16, 2526–2530.
Gepner, A.D., Piper, M.E., Johnson, H.M., Fiore, M.C., Baker, T.B., Stein, J.H., 2011. Effects of smoking and smoking cessation on lipids and lipoproteins: outcomes from a randomized clinical trial. Am. Heart J. 161, 145–151.
Glassberg, M.K., Catanuto, P., Shahzeidi, S., Aliniazee, M., Lilo, S., Rubio, G.A., Elliot, S.J., 2016. Estrogen deficiency promotes cigarette smoke-induced changes in the extracellular matrix in the lungs of aging female mice. Transl. Res. 178, 107–117.
Goldklang, M., Golovatch, P., Zelonina, T., Trischler, J., Rabinowitz, D., Lemaitre, V., D'Armiento, J., 2012. Activation of the TLR4 signaling pathway and abnormal cholesterol efflux lead to emphysema in ApoE-deficient mice. Am. J. Physiol. Lung Cell Mol. Physiol. 302, L1200–L1208.
Grundy, S.M., Cleeman, J.I., Merz, C.N., Brewer Jr., H.B., Clark, L.T., Hunninghake, D.B., Pasternak, R.C., Smith Jr., S.C., Stone, N.J., National Heart, L., Blood, I., American College of Cardiology, F., American Heart, A, 2004. Implications of recent clinical trials for the national cholesterol education program adult treatment panel III guidelines. Circulation 110, 227–239.
Hamm, J.T., Yee, S., Rajendran, N., Morrissey, R.L., Richter, S.J., Misra, M., 2007. Histological alterations in male A/J mice following nose-only exposure to tobacco smoke. Inhal. Toxicol. 19, 405–418.
Health Canada, 2000. Tobacco Products Information Regulations. https://www.canada.ca/en/health-canada/services/health-concerns/reports-publications/tobacco/tobacco-products-information-regulations.html, Accessed date: 14 February 2019.
Hellerstein, M.K., Benowitz, N.L., Neese, R.A., Schwartz, J.M., Hoh, R., Jacob 3rd, P., Hsieh, J., Faix, D., 1994. Effects of cigarette smoking and its cessation on lipid metabolism and energy expenditure in heavy smokers. J. Clin. Invest. 93, 265–272.
Hoeng, J., Deehan, R., Pratt, D., Martin, F., Sewer, A., Thomson, T.M., Drubin, D.A., Waters, C.A., de Graaf, D., Peitsch, M.C., 2012. A network-based approach to quantifying the impact of biologically active substances. Drug Discov. Today 17, 413–418.
Hofstetter, A., Schutz, Y., Jequier, E., Wahren, J., 1986. Increased 24-hour energy expenditure in cigarette smokers. N. Engl. J. Med. 314, 79–82.
Kilaru, S., Frangos, S.G., Chen, A.H., Gortler, D., Dhadwal, A.K., Araim, O., Sumpio, B.E., 2001. Nicotine: a review of its role in atherosclerosis. J. Am. Coll. Surg. 193, 538–546.
Kogel, U., Schlage, W.K., Martin, F., Xiang, Y., Ansari, S., Leroy, P., Vanscheeuwijck, P., Gebel, S., Buettner, A., Wyss, C., Esposito, M., Hoeng, J., Peitsch, M.C., 2014. A 28-day rat inhalation study with an integrated molecular toxicology endpoint demonstrates reduced exposure effects for a prototypic modified risk tobacco product compared with conventional cigarettes. Food Chem. Toxicol. 68, 204–217.
Laniado-Laborin, R., 2009. Smoking and chronic obstructive pulmonary disease (COPD). Parallel epidemics of the 21 century. Int. J. Environ. Res. Public Health 6, 209–224.
Li, Y., Yu, G., Yuan, S., Tan, C., Lian, P., Fu, L., Hou, Q., Xu, B., Wang, H., 2017. Cigarette smoke-induced pulmonary inflammation and autophagy are attenuated in ephx2-deficient mice. Inflammation 40, 497–510.
Lietz, M., Berges, A., Lebrun, S., Meurrens, K., Steffen, Y., Stolle, K., Schueller, J., Boue, S., Vuillaume, G., Vanscheeuwijck, P., Moehring, M., Schlage, W., De Leon, H., Hoeng, J., Peitsch, M., 2013. Cigarette-smoke-induced atherogenic lipid profiles in plasma and vascular tissue of apolipoprotein E-deficient mice are attenuated by smoking cessation. Atherosclerosis 229, 86–93.
Lo Sasso, G., Schlage, W.K., Boue, S., Veljkovic, E., Peitsch, M.C., Hoeng, J., 2016. The Apoe(-/-) mouse model: a suitable model to study cardiovascular and respiratory diseases in the context of cigarette smoke exposure and harm reduction. J. Transl. Med. 14, 146.
March, T.H., Wilder, J.A., Esparza, D.C., Cossey, P.Y., Blair, L.F., Herrera, L.K., McDonald, J.D., Campen, M.J., Mauderly, J.L., Seagrave, J., 2006. Modulators of cigarette smoke-induced pulmonary emphysema in A/J mice. Toxicol. Sci. 92, 545–559.
Martin, F., Sewer, A., Talikka, M., Xiang, Y., Hoeng, J., Peitsch, M.C., 2014. Quantification of biological network perturbations for mechanistic insight and diagnostics using two-layer causal models. BMC Bioinf. 15, 238.
Martin, F., Thomson, T.M., Sewer, A., Drubin, D.A., Mathis, C., Weisensee, D., Pratt, D., Hoeng, J., Peitsch, M.C., 2012. Assessment of network perturbation amplitude by applying high-throughput data to causal biological networks. BMC Syst. Biol. 6, 54.
Massaro, D., Massaro, G.D., 2008. Apoetm1Unc mice have impaired alveologenesis, low lung function, and rapid loss of lung function. Am. J. Physiol. Lung Cell Mol. Physiol. 294, L991–L997.
Murphy, J., Gaca, M., Lowe, F., Minet, E., Breheny, D., Prasad, K., Camacho, O., Fearon, I.M., Liu, C., Wright, C., McAdam, K., Proctor, C., 2017. Assessing modified risk tobacco and nicotine products: description of the scientific framework and assessment of a closed modular electronic cigarette. Regul. Toxicol. Pharmacol. 90, 342–357.
NACLAR, 2004. Guidelines on the Care and Use of Animals for Scientific Purposes. https://www.ava.gov.sg/docs/default-source/tools-and-resources/resources-for-businesses/attach3_animalsforscientificpurposes, Accessed date: 14 February 2019.
Niaura, R., 2016. Re-thinking Nicotine and its Effects. https://truthinitiative.org/sites/default/files/ReThinking-Nicotine.pdf.
Phillips, B., Schlage, W.K., Titz, B., Kogel, U., Sciuscio, D., Martin, F., Leroy, P., Vuillaume, G., Krishnan, S., Lee, T., Veljkovic, E., Elamin, A., Merg, C., Ivanov, N.V., Peitsch, M.C., Hoeng, J., Vanscheeuwijck, P., June 2018. A 90-day OECD TG 413 rat inhalation study with systems toxicology endpoints demonstrates reduced exposure effects of the aerosol from the carbon heated tobacco product version 1.2 (CHTP1.2) compared with cigarette smoke. I. Inhalation exposure, clinical pathology and histopathology. Food Chem. Toxicol. 116 (Part B), 388–413.
Phillips, B., Veljkovic, E., Boue, S., Schlage, W.K., Vuillaume, G., Martin, F., Titz, B., Leroy, P., Buettner, A., Elamin, A., Oviedo, A., Cabanski, M., De Leon, H., Guedj, E., Schneider, T., Talikka, M., Ivanov, N.V., Vanscheeuwijck, P., Peitsch, M.C., Hoeng, J., 2016. An 8-month systems toxicology inhalation/cessation study in apoe-/- mice to investigate cardiovascular and respiratory exposure effects of a candidate modified risk tobacco product, THS 2.2, compared with conventional cigarettes. Toxicol. Sci. 149, 411–432.
Phillips, B., Veljkovic, E., Peck, M.J., Buettner, A., Elamin, A., Guedj, E., Vuillaume, G., Ivanov, N.V., Martin, F., Boue, S., Schlage, W.K., Schneider, T., Titz, B., Talikka, M., Vanscheeuwijck, P., Hoeng, J., Peitsch, M.C., 2015. A 7-month cigarette smoke inhalation study in C57BL/6 mice demonstrates reduced lung inflammation and emphysema following smoking cessation or aerosol exposure from a prototypic modified risk tobacco product. Food Chem. Toxicol. 80, 328–345.
Rahman, I., Kilty, I., 2006. Antioxidant therapeutic targets in COPD. Curr. Drug Targets 7, 707–720.
Rangasamy, T., Cho, C.Y., Thimmulappa, R.K., Zhen, L., Srisuma, S.S., Kensler, T.W., Yamamoto, M., Petrache, I., Tuder, R.M., Biswal, S., 2004. Genetic ablation of Nrf2 enhances susceptibility to cigarette smoke-induced emphysema in mice. J. Clin. Invest. 114, 1248–1259.
Rangasamy, T., Misra, V., Zhen, L., Tankersley, C.G., Tuder, R.M., Biswal, S., 2009. Cigarette smoke-induced emphysema in A/J mice is associated with pulmonary oxidative stress, apoptosis of lung cells, and global alterations in gene expression. Am. J. Physiol. Lung Cell Mol. Physiol. 296, L888–L900.
Rao Ch, S., Subash, Y.E., 2013. The effect of chronic tobacco smoking and chewing on the lipid profile. J. Clin. Diagn. Res. 7, 31–34.
Royal College of Physicians, 2007. Harm Reduction in Nicotine Addiction Helping People Who Can't Quit. A Report by the Tobacco Advisory Group of the Royal College of Physicians.
Royal College of Physicians, 2016. Nicotine without Smoke Tobacco Harm Reduction. A Report by the Tobacco Advisory Group of the Royal College of Physicians.
Saetta, M., Turato, G., Maestrelli, P., Mapp, C.E., Fabbri, L.M., 2001. Cellular and structural bases of chronic obstructive pulmonary disease. Am. J. Respir. Crit. Care Med. 163, 1304–1309.
Santanam, N., Thornhill, B.A., Lau, J.K., Crabtree, C.M., Cook, C.R., Brown, K.C., Dasgupta, P., 2012. Nicotinic acetylcholine receptor signaling in atherogenesis. Atherosclerosis 225, 264–273.
Schaller, J.P., Keller, D., Poget, L., Pratte, P., Kaelin, E., McHugh, D., Cudazzo, G., Smart, D., Tricker, A.R., Gautier, L., Yerly, M., Reis Pires, R., Le Bouhellec, S., Ghosh, D., Hofer, I., Garcia, E., Vanscheeuwijck, P., Maeder, S., 2016. Evaluation of the Tobacco Heating System 2.2. Part 2: chemical composition, genotoxicity, cytotoxicity, and physical properties of the aerosol. Regul. Toxicol. Pharmacol. 81 (Suppl 2), S27–S47.
Scherle, W., 1970. A simple method for volumetry of organs in quantitative stereology. Mikroskopie 26, 57–60.
Seagrave, J., Barr, E.B., March, T.H., Nikula, K.J., 2004. Effects of cigarette smoke exposure and cessation on inflammatory cells and matrix metalloproteinase activity in mice. Exp. Lung Res. 30, 1–15.
Serrano, M., Madoz, E., Ezpeleta, I., San Julian, B., Amezqueta, C., Perez Marco, J.A., de Irala, J., 2003. [Smoking cessation and risk of myocardial reinfarction in coronary patients: a nested case-control study]. Rev. Esp. Cardiol. 56, 445–451.
Sharafkhaneh, A., Hanania, N.A., Kim, V., 2008. Pathogenesis of emphysema: from the bench to the bedside. Proc. Am. Thorac. Soc. 5, 475–477.
Shen, Y., Yue, F., McCleary, D.F., Ye, Z., Edsall, L., Kuan, S., Wagner, U., Dixon, J., Lee, L., Lobanenkov, V.V., Ren, B., 2012. A map of the cis-regulatory sequences in the mouse genome. Nature 488, 116–120.
Smith, M.R., Clark, B., Ludicke, F., Schaller, J.P., Vanscheeuwijck, P., Hoeng, J., Peitsch, M.C., 2016. Evaluation of the tobacco heating system 2.2. Part 1: description of the system and the scientific assessment program. Regul. Toxicol. Pharmacol. 81 (Suppl. 2), S17–S26.
Stadler, M.B., Murr, R., Burger, L., Ivanek, R., Lienert, F., Scholer, A., van Nimwegen, E., Wirbelauer, C., Oakeley, E.J., Gaidatzis, D., Tiwari, V.K., Schubeler, D., 2011. DNA-binding factors shape the mouse methylome at distal regulatory regions. Nature 480, 490–495.
Stinn, W., Arts, J.H., Buettner, A., Duistermaat, E., Janssens, K., Kuper, C.F., Haussmann, H.J., 2010. Murine lung tumor response after exposure to cigarette mainstream smoke or its particulate and gas/vapor phase fractions. Toxicology 275, 10–20.
Stinn, W., Buettner, A., Weiler, H., Friedrichs, B., Luetjen, S., van Overveld, F., Meurrens, K., Janssens, K., Gebel, S., Stabbert, R., Haussmann, H.J., 2013. Lung inflammatory effects, tumorigenesis, and emphysema development in a long-term inhalation study with cigarette mainstream smoke in mice. Toxicol. Sci. 131, 596–611.
Szostak, J., Boue, S., Talikka, M., Guedj, E., Martin, F., Phillips, B., Ivanov, N.V., Peitsch, M.C., Hoeng, J., 2017. Aerosol from Tobacco Heating System 2.2 has reduced impact on mouse heart gene expression compared with cigarette smoke. Food Chem. Toxicol. 101, 157–167.
Tam, A., Bates, J.H., Churg, A., Wright, J.L., Man, S.F., Sin, D.D., 2016a. Sex-related differences in pulmonary function following 6 Months of cigarette exposure: implications for sexual dimorphism in mild COPD. PLoS One 11, e0164835.
Tam, A., Churg, A., Wright, J.L., Zhou, S., Kirby, M., Coxson, H.O., Lam, S., Man, S.F., Sin, D.D., 2016b. Sex differences in airway remodeling in a mouse model of chronic obstructive pulmonary disease. Am. J. Respir. Crit. Care Med. 193, 825–834.
Taylor Jr., D.H., Hasselblad, V., Henley, S.J., Thun, M.J., Sloan, F.A., 2002. Benefits of smoking cessation for longevity. Am. J. Public Health 92, 990–996.
Terpstra, P.M., Teredesai, A., Vanscheeuwijck, P.M., Verbeeck, J., Schepers, G., Radtke, F., Kuhl, P., Gomm, W., Anskeit, E., Patskan, G., 2003. Toxicological evaluation of an electrically heated cigarette. Part 4: subchronic inhalation toxicology. J. Appl. Toxicol. 23, 349–362.
Thatcher, T.H., McHugh, N.A., Egan, R.W., Chapman, R.W., Hey, J.A., Turner, C.K., Redonnet, M.R., Seweryniak, K.E., Sime, P.J., Phipps, R.P., 2005. Role of CXCR2 in cigarette smoke-induced lung inflammation. Am. J. Physiol. Lung Cell Mol. Physiol. 289, L322–L328.
Titz, B., Kogel, U., Martin, F., Schlage, W.K., Xiang, Y., Nury, C., Dijon, S., Baumer, K., Peric, D., Bornand, D., Dulize, R., Phillips, B., Leroy, P., Vuillaume, G., Lebrun, S., Elamin, A., Guedj, E., Trivedi, K., Ivanov, N.V., Vanscheeuwijck, P., Peitsch, M.C.,

Hoeng, J., 2018. A 90-day OECD TG 413 rat inhalation study with systems toxicology endpoints demonstrates reduced exposure effects of the aerosol from the carbon heated tobacco product version 1.2 (CHTP1.2) compared with cigarette smoke. II. Systems toxicology assessment. Food Chem. Toxicol. 115, 284–301.

Tricker, A.R., Kanada, S., Takada, K., Leroy, C.M., Lindner, D., Schorp, M.K., Dempsey, R., 2012. Reduced exposure evaluation of an electrically heated cigarette smoking system. Part 5: 8-day randomized clinical trial in Japan. Regul. Toxicol. Pharmacol 64, S54–S63.

Tuder, R.M., McGrath, S., Neptune, E., 2003. The pathobiological mechanisms of emphysema models: what do they have in common? Pulm. Pharmacol. Therapeut. 16, 67–78.

Vizcaino, J.A., Deutsch, E.W., Wang, R., Csordas, A., Reisinger, F., Rios, D., Dianes, J.A., Sun, Z., Farrah, T., Bandeira, N., Binz, P.A., Xenarios, I., Eisenacher, M., Mayer, G., Gatto, L., Campos, A., Chalkley, R.J., Kraus, H.J., Albar, J.P., Martinez-Bartolome, S., Apweiler, R., Omenn, G.S., Martens, L., Jones, A.R., Hermjakob, H., 2014. ProteomeXchange provides globally coordinated proteomics data submission and dissemination. Nat. Biotechnol. 32, 223–226.

Wang, C., Chen, H., Zhu, W., Xu, Y., Liu, M., Zhu, L., Yang, F., Zhang, L., Liu, X., Zhong, Z., Zhao, J., Jiang, J., Xiang, M., Yu, H., Hu, X., Lu, H., Wang, J., 2017. Nicotine accelerates atherosclerosis in apolipoprotein E-deficient mice by activating alpha7 nicotinic acetylcholine receptor on mast cells. Arterioscler. Thromb. Vasc. Biol. 37, 53–65.

Werley, M.S., Freelin, S.A., Wrenn, S.E., Gerstenberg, B., Roemer, E., Schramke, H., Van Miert, E., Vanscheeuwijck, P., Weber, S., Coggins, C.R., 2008. Smoke chemistry, in vitro and in vivo toxicology evaluations of the electrically heated cigarette smoking system series K. Regul. Toxicol. Pharmacol. 52, 122–139.

Wu, X., Zhang, H., Qi, W., Zhang, Y., Li, J., Li, Z., Lin, Y., Bai, X., Liu, X., Chen, X., Yang, H., Xu, C., Zhang, Y., Yang, B., 2018. Nicotine promotes atherosclerosis via ROS-NLRP3-mediated endothelial cell pyroptosis. Cell Death Dis. 9, 171.

Yang, S.R., Chida, A.S., Bauter, M.R., Shafiq, N., Seweryniak, K., Maggirwar, S.B., Kilty, I., Rahman, I., 2006. Cigarette smoke induces proinflammatory cytokine release by activation of NF-kappaB and posttranslational modifications of histone deacetylase in macrophages. Am. J. Physiol. Lung Cell Mol. Physiol. 291, L46–L57.

Yusuf, S., Hawken, S., Ounpuu, S., Dans, T., Avezum, A., Lanas, F., McQueen, M., Budaj, A., Pais, P., Varigos, J., Lisheng, L., Investigators, I.S., 2004. Effect of potentially modifiable risk factors associated with myocardial infarction in 52 countries (the INTERHEART study): case-control study. Lancet 364, 937–952.

Zanetti, F., Titz, B., Sewer, A., Lo Sasso, G., Scotti, E., Schlage, W.K., Mathis, C., Leroy, P., Majeed, S., Torres, L.O., Keppler, B.R., Elamin, A., Trivedi, K., Guedj, E., Martin, F., Frentzel, S., Ivanov, N.V., Peitsch, M.C., Hoeng, J., 2017. Comparative systems toxicology analysis of cigarette smoke and aerosol from a candidate modified risk tobacco product in organotypic human gingival epithelial cultures: a 3-day repeated exposure study. Food Chem. Toxicol. 101, 15–35.

Zheng, L., Park, J., Walls, M., Tully, M., Jannasch, A., Cooper, B., Shi, R., 2013. Determination of urine 3-HPMA, a stable acrolein metabolite in a rat model of spinal cord injury. J. Neurotrauma 30, 1334–1341.